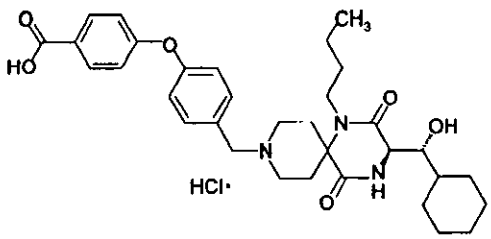

FIG. 1. Structure of AK602.

MATERIALS AND METHODS

Transplantation of human PBMC in NOG mice. NOD-SCID (NOG) mice (10, 33) were maintained in the Central Institute for Experimental Animals (Kawasaki, Japan). Mice were 4 to 6 weeks old at the time of transfer of human PBMC. The human PBMC-transplanted NOG (hu-PBMC-NOG) mice were generated by methods previously described (23, 24). Briefly, PBMC (10^7) were freshly prepared from heparinized blood of a single healthy HIV-1-seronegative donor by Ficoll-Hypaque density gradient centrifugation, resuspended in RPMI 1640-based culture medium (0.5 ml), and infused intraperitoneally to each mouse. The experimental protocol was approved by the Ethics Review Committees for Animal Experimentation of the participating institutions.

Assay for proliferation and CCR5 expression of transplanted human PBMC recovered from hu-PBMC-NOG mice. Freshly isolated human PBMC (2×10^7 cells/ml) were incubated in phosphate-buffered saline (PBS) containing 10 μM 5-carboxyfluorescein diacetate succinimidyl ester (CFSE; Molecular Probes, Eugene, Oreg.) for 15 min at 37°C for CFSE labeling as previously described by Lyons (16), washed, and resuspended in RPMI 1640. One part of the labeled PBMC preparation was intraperitoneally injected (10^7 PBMC) to each NOG mouse, and human PBMC were recovered from peritoneal lavages and spleen. The other part of the preparation was immediately stimulated with 10 μg of phytohemagglutinin (PHA)/ml, cultured, and harvested. PBMC samples thus obtained were labeled with phycoerythrin (PE)-conjugated anti-CCR5 monoclonal antibody 3A9 or peridinin chlorophyll protein-conjugated anti-HLA-DR antibody (BD Pharmingen, San Diego, Calif.) and subjected to flow cytometric analysis with a Becton Dickinson FACscan cytometer; the data were analyzed by Cell Quest software (Becton Dickinson, Franklin Lakes, N.J.). A quantitative fluorescence-activated cell sorting (FACS) assay that relies on a series of precalibrated beads that bind to a fixed number of mouse immunoglobulin G molecules (Quantum Simply Cellular Kit; Sigma, Saint Louis, Mo.) to determine the absolute number of CCR5s on the cell surface was also conducted according to the manufacturer's instructions (15).

Cells and viruses. The HeLa-CD4-LTR-β-gal indicator cell line expressing human CCR5 ($CCR5^+$ MAGI) (18), a kind gift from Yosuke Maeda, was used for the present study. 293T cells (a human embryonic kidney cell line) were cultured in Dulbecco's modified Eagle medium supplemented with 10% fetal calf serum (FCS) and antibiotics and used for transfection of DNA plasmid containing the R5 HIV-$1_{JR\text{-}FL}$ genome (13). PBMC isolated from HIV-1-seronegative individuals were cultured with 10% FCS and antibiotics with 10 μg of PHA/ml for 3 days prior to anti-HIV-1 activity assay in vitro (PHA-PBMC). A panel of HIV-1 strains was employed for the drug susceptibility attempt: HIV-$1_{Ba\text{-}L}$ (7), HIV-$1_{JR\text{-}FL}$ (13), HIV-$1_{NL4\text{-}3}$ (32), a wild-type HIV-1_{MOKW} isolated from a drug-naive AIDS patient (17), and MDR primary HIV-1 (HIV-1_{MDR}) strain (HIV-1_{JSL} and HIV-1_{MM}) (35). All primary HIV-1 strains were passaged once or twice in PHA-PBMC cultures and the culture supernatants were stored at −80°C until use. Antiviral assays using PHA-PBMC were conducted as previously reported (12, 17, 35).

Antiviral agents and assay for inhibition of R5 HIV-1 infectivity and replication. A series of different spirodiketopiperazine (SDP) derivatives were newly designed, synthesized, and tested for their activity against in vitro infectivity and replication of R5 HIV-1 as previously described (17). AK602 was chosen for this study based on its CCR5-specific, potent activity against R5 HIV-1. A method for the synthesis of AK602 will be published elsewhere. The structure of AK602 is illustrated in Fig. 1. An approved drug for therapy for HIV-1 infection, 2′,3′-dideoxyinosine (ddI) (20, 21), was kindly provided by Ajinomoto Co., Inc. Tokyo, Japan. TAK779 and SCH-C were synthesized according to previously published data (1, 30). The MAGI assay using $CCR5^+$ MAGI cells was conducted as previously described (17) with minor modifications. Briefly, $CCR5^+$ MAGI cells were seeded in 96-well, flat-bottomed microculture plates (10^4 cells/well) for 24 h, exposed to 0.1 or 1 μM AK602 for 30 min, washed three times, exposed to R5 HIV-1 (100 50% tissue culture infectious doses) at various time points after AK602 removal, and cultured in Dulbecco's modified Eagle medium containing 15% FCS for 48 h. Following the removal of supernatants and lysis of the cells with PBS (100 μl) containing 1% Triton X-100, a solution (100 μl) containing 10 mM chlorophenol red-β-D-galactopyranoside, 2 mM $MgCl_2$, and 0.1 M KH_2PO_4 was added to each well; the mixture was incubated at room temperature in the dark for 30 min; and the optical density (wavelength, 570 nm) was measured with a microplate reader (*V*max, Molecular Devices, Sunnyvale, Calif). All assays were performed in triplicate.

Pharmacokinetic analysis of AK602 in hu-PBMC-NOG mice. Pharmacokinetic analysis of AK602 in hu-PBMC-NOG mice was performed as previously described (28). In brief, plasma samples were collected periodically over 12 h following a single AK602 administration at a dose of 60 mg/kg of body weight dissolved in 400 μl of 4% hydroxypropyl-β cyclodextrin (HPBC). Each plasma sample (150 μl) was centrifuged at 3,000 rpm for 10 min, and the supernatant was vacuum concentrated and injected into the high-performance liquid chromatography (HPLC) system. The eluent was monitored at 255 nm of UV, and the AK602 concentration in plasma was determined.

Determination of amounts of AK602 persistently bound to CCR5 in hu-PBMC-NOG mice. Blood samples were collected from the tail vein of each hu-PBMC-NOG mouse at various time points following a single intraperitoneal administration of AK602 at a dose of 60 mg/kg. PBMC were isolated by density gradient centrifugation and stained with fluorescein isothiocyanate-conjugated monoclonal antibody 45531 (R&D Systems, Minneapolis, Minn.) specific for the C-terminal half of the second extracellular loop (ECL2B) of CCR5 (15) known to be competitively replaced by SDP derivatives (17) or with PE-conjugated monoclonal antibody 3A9, which binds to the N-terminus extracellular domain of CCR5 (17). PBMC were then subjected to FACS analysis.

Treatment of R5 HIV-1-infected hu-PBMC-NOG mice with anti-HIV-1 agents. Sixteen days after PBMC infusion, the mice were bled from the tail vein, and three-color flow cytometric analysis was performed to confirm positive engraftment of human HLA, CD4, and CD8 antigens on the cells recovered. HIV-$1_{JR\text{-}FL}$ (2,000 50% tissue culture infectious doses) was intraperitoneally inoculated to each mouse in which PBMC engraftment was confirmed. Twenty-four hours after the R5 HIV-1 inoculation, administration of AK602 (120 mg in 4% HPBC/kg/day, twice a day), ddI (50 mg in 4% HPBC/kg/day, twice a day), or saline was implemented and continued by day 16. On days 5 and 9 after the R5 HIV-1 inoculation, blood samples were collected from mouse tail veins for immunologic and virological monitoring (see below). On day 16, blood samples were collected by cardiocentesis, and the mice were sacrificed. The experimental protocol for the treatment is illustrated in Fig. 2.

Immunologic and virological monitoring. Human PBMC recovered from mice were subjected to immunologic and virological monitoring as previously described (23, 24). The $CD4^+/CD8^+$ cell ratios were determined by FACS analysis with PE-conjugated mouse anti-CD4 and peridinin chlorophyll protein-conjugated mouse anti-CD8 (BD Pharmingen) monoclonal antibodies. Determination of HIV-1 DNA copy numbers in recovered human PBMC was performed by real-time PCR assay with Taqman Master mixture (PE Biosystems) and HIV long terminal repeat-specific primers M667 (5′-GGC TAA CTA GGG AAC CCA CTG-3′) and AA55 (5′-CTG CTA GAG ATT TTC CAC ACT GAC-3′). HIV-1-specific products were quantified with the ABI 7700 detection system (Applied Biosystems, Foster City, Calif.), and cell numbers were determined with the RAG-1 gene. The numbers of $CD4^+$ cells were calculated based on the percentage of $CD4^+$ values obtained from the FACS analysis of each test PBMC sample, and R5 HIV-1 proviral DNA copy numbers were expressed as copy numbers per 10^5 $CD4^+$ cells. In some experiments, $CD4^+$ and $CD4^-$ cells were separated before real-time PCR assay with the rapid immunomagnetic CD4-positive cell isolation kit (Dynabeads M-450 CD4; Dynal Biotech, Inc., Lake

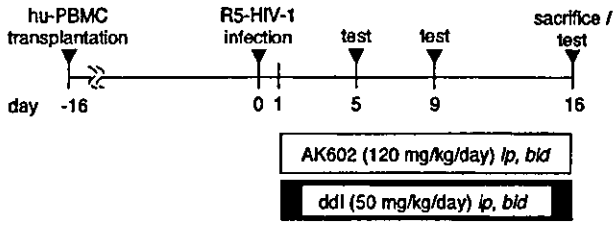

FIG. 2. Protocol for drug administration and immunological and virologic monitoring.

Success, N.Y.). The amounts of p24 antigen in murine sera were determined using a fully automated chemiluminescent enzyme immunoassay system (Lumipulse F; Fujirebio, Inc., Tokyo, Japan) as previously described (12). Plasma viral load was quantified with the AMPLICOR HIV-1 monitor test kit, version 1.5 (Roche Diagnostics, Branchburg, N.J.).

Statistical analyses. Nonparametric statistical analyses were performed by using the Mann-Whitney U test (Statview, version 5.0; Abacus Concepts, Berkeley, Calif.). The difference between viremia levels in two groups of mice was determined by the Wilcoxon rank sum test. For each mouse, the value of $\log_{10}$ RNA copies was calculated, and the slope corresponding to the rate of increase per day was determined by simple linear regression for the days (5, 9, and 16) of blood collection. The resulting slopes for all mice in the untreated groups were compared to the slopes of mice in each of the other two groups.

RESULTS

Transplanted PBMC in hu-PBMC-NOG mice are intensely activated and express high levels of CCR5. When we examined the proliferation profile of PBMC stimulated with PHA in vitro by treatment with the vital dye CFSE, which allows the analysis of cell proliferation as the CFSE's fluorescence intensity is halved per each cell division, there was only a slight shift to the left in the flow cytometric profile on days 1 and 2 of culture (Fig. 3A). On day 4 of culture, a discrete shift to the left was identified, suggesting that the PHA-PBMC underwent up to four cycles of proliferation in vitro by day 4. In contrast, PBMC transplanted and recovered on day 2 had apparently undergone ~4 cycles of proliferation; by day 4, a majority of cells had undergone up to 10 cycles and beyond in proliferation (Fig. 3B). It was possible that the CFSE-negative and weakly CFSE-positive cells which accumulated on days 2 and 4 (Fig. 3B) were murine cells that engulfed and degraded CFSE. We therefore conducted experiments in which the cells with CFSE dilution were directly confirmed to be human CCR5-positive cells. As can be seen in Fig. 3C, when cells were recovered from the spleen of an NOG mouse into which CFSE-labeled PBMC had been transplanted and stained with monoclonal antibody 45531, which is specific for the C-terminal half of the second extracellular loop (ECL2B) of CCR5 (15), the majority of such human $CCR5^+$ cells proved to be CFSE negative. We also examined the levels of cellular activation by the expression of HLA-DR on cell surface. The levels of HLA-DR expression in PBMC recovered from uninfected NOG mice 3 days after transplantation were much greater than those in 3-day-cultured PBMC following PHA stimulation (Fig. 3D). The fluorescence intensity in the same donor's PHA-PBMC examined on three different occasions was 21 ± 4, while that of the PBMC recovered from mice was 91 ± 25 (Fig. 3D). When we further assessed the levels of CCR5 expression, the PBMC recovered from the mice on day 3 proved to be strongly positive for CCR5 (Fig. 3E). The CCR5-positive fraction in the PBMC recovered was 49.7%, while that in PHA-PBMC was 27.3%. The mean fluorescence intensity of the $CCR5^+$ cell population was 141, compared to the $CCR5^+$ cell population in PHA-PBMC with a mean fluorescence intensity of 51. The estimated number of CCR5 expressed on the PBMC recovered on day 3 was 25,348 (as antibody binding sites per cell) while that on PHA-PBMC on day 3 in culture was 8,981 antibody binding sites as examined by quantitative FACS assay. These data indicate that the transplanted human PBMC were intensely activated and rapidly proliferating and expressed high levels of CCR5 on their cell surfaces.

Potent activity of AK602 against R5 HIV-1 in vitro. Among SDP derivatives we designed and synthesized, AK602 was identified to be highly potent against a broad spectrum of R5 HIV-1 strains, including MDR clinical R5 HIV-1 isolates in vitro with 50% inhibitory concentration (IC_{50}) values of 0.3 to 0.6 nM, although two previously published CCR5 antagonists (TAK779 and SCH-C) were substantially less potent than AK602 (Table 1). AK602 and other CCR5 antagonists failed to inhibit the replication of an X4 HIV-1 strain, HIV-1_{NL4-3}.

Pharmacokinetics of AK602 in hu-PBMC-NOG mice. We examined the pharmacokinetics of AK602 in hu-PBMC-NOG mice by intraperitoneally administering the compound at a dose of 60 mg/kg. Plasma samples were collected periodically up to 12 h and subjected to HPLC analysis. As shown in Fig. 4A, the concentration of AK602 reached the maximal concentration immediately after intraperitoneal administration and decreased rapidly. The calculated plasma half-life in the α-phase of the concentration curve was as short as 29 min.

AK602 persists on cell surface CCR5. As shown above, the plasma half-life of AK602 turned out to be short; however, considering that AK602 possesses such a high affinity to CCR5 and potent activity against R5 HIV-1 in vitro, it was thought possible that AK602 would remain attached on cellular CCR5 for an extensive period of time and exert anti-R5 HIV-1 activity even when the compound was depleted from circulation. To examine this possibility, we used two monoclonal antibodies, 45531 and 3A9. When human PBMC were recovered from a hu-PBMC-NOG mouse 2 and 6 h after AK602 administration (60 mg/kg) and stained with 45531, AK602 proved to block the binding of 45531 to CCR5 (Fig. 4B), while AK602 failed to block 3A9 binding to CCR5 (Fig. 4C), suggesting that AK602 did not elicit CCR5 internalization or shedding at all at least for 6 h. We subsequently examined whether AK602 remained on cellular CCR5 with the 45531 monoclonal antibody. When the cells were recovered from mice 2, 6, and 14 h after the AK602 administration, the mean values of the percentage of AK602 occupancy were 85 (four mice), 54 (three mice), and 16 (three mice), respectively. It was calculated that it took about 9 h for AK602 occupancy to be reduced by 50% (Fig. 4D).

Anti-R5 HIV-1 activity of AK602 persistently seen after its removal from culture medium. In another depletion experiment, we exposed $CCR5^+$ MAGI cells to AK602 for 30 min, depleted the compound from the culture by thorough washing, incubated the cells for various lengths of time, exposed the cells to HIV-1_{Ba-L}, further cultured the cells for 48 h, and determined whether HIV-1_{Ba-L} infection was blocked by AK602 exposure (Fig. 4E). When the $CCR5^+$ MAGI cells were exposed to 0.1 and 1 μM AK602 and exposed to HIV-1_{Ba-L} immediately afterward, the values for protection were 68 and 85%, respectively. When the cells were exposed to HIV-1_{Ba-L} 4 h after depletion, 49 and 72% of the cells were protected by 0.1 and 1 μM AK602. When the cells were exposed to HIV-1_{Ba-L} 12 and 24 h after depletion, 57 and 45% of the cells were seen protected by 1 μM, respectively (Fig. 4E).

Effects of AK602 on $CD4^+$ and $CD8^+$ cell counts in R5 HIV-1-infected hu-PBMC-NOG mice. PBMC were recovered from murine blood samples collected on days 5, 9, and 16 after R5 HIV-1 inoculation and subjected to flow cytometric analysis for determination of $CD4^+/CD8^+$ cell ratios. As shown in Fig. 5A, in PBMC recovered on day 16 from a representative

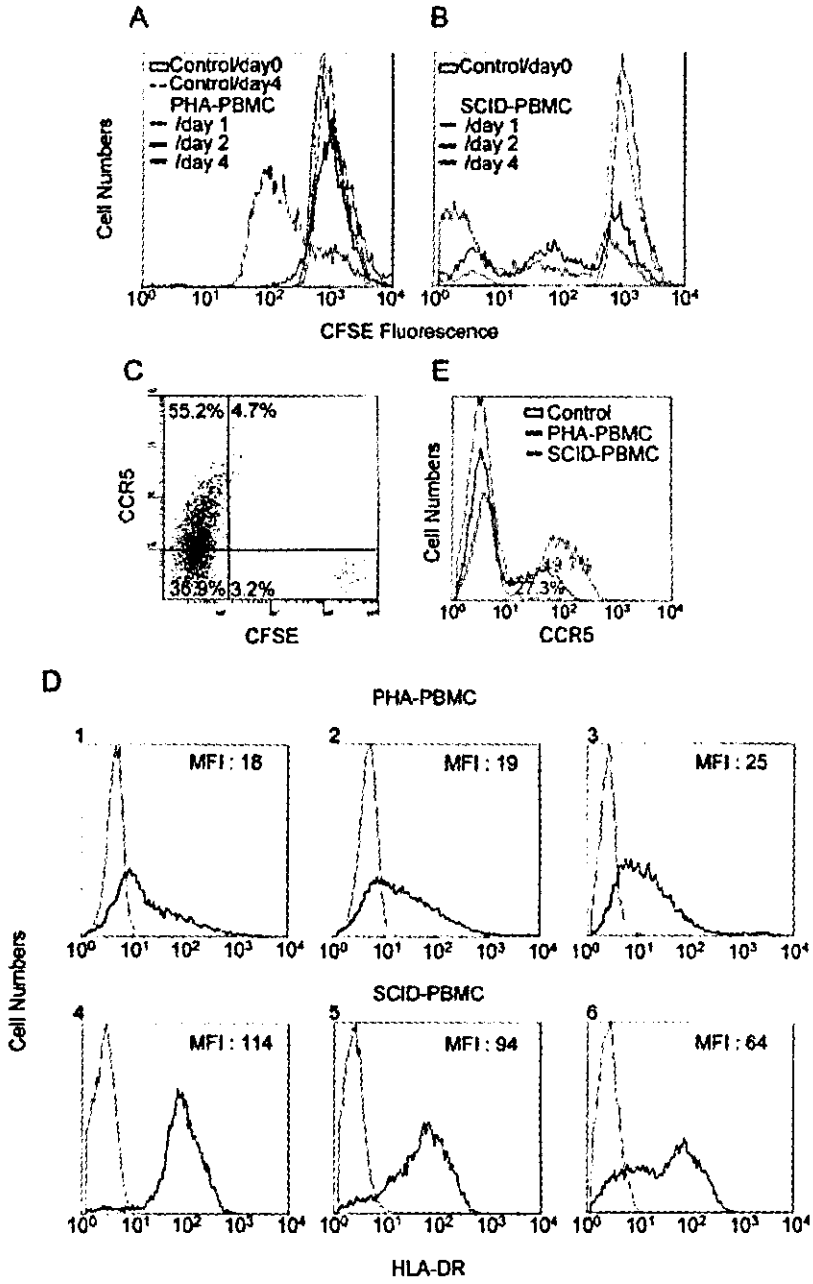

FIG. 3. Transplanted PBMC are intensely activated and express high levels of CCR5. (A and B) Proliferation profiles of PHA-PBMC and transplanted and recovered PBMC. Freshly prepared PBMC were incubated with the vital dye CFSE, and one part of such PBMC preparation was stimulated with PHA, while the other part was intraperitoneally transplanted to mice. On days 1, 2, and 4, the cells were harvested and the fluorescence intensity of CFSE was determined. Note that transplanted PBMC recovered on day 2 had undergone ~4 cycles of proliferation; by day 4, a majority of cells had undergone ~10 cycles and more of proliferation. (C) CCR5 expression level and CFSE intensity in human PBMC harvested from a spleen of hu-PBMC-NOG mouse on day 4. (D) Intense activation of PBMC after transplantation. PBMC stimulated with PHA and cultured for 4 days (panels 1 to 3) and transplanted PBMC recovered from the uninfected mice on day 4 (panels 4 to 6) were stained with an anti-HLA-DR monoclonal antibody. Note that HLA-DR expression levels in transplanted PBMC were much higher than those in PHA-PBMC. (E) CCR5 expression profiles of PHA-PBMC and transplanted PBMC. PBMC stimulated with PHA and cultured for 3 days and transplanted PBMC recovered from the uninfected mice on day 3 were stained with PE-conjugated anti-CCR5 monoclonal antibody 3A9 and subjected to flow cytometric analysis. SCID-PBMC, PBMC transplanted and recovered.

R5 HIV-1-infected, saline-treated mouse, there were only few $CD4^+$ cells (3.9% [1.4% + 2.5%]) resulting in a $CD4^+/CD8^+$ cell ratio of 0.05. However, a distinct $CD4^+$ cell population (55.1% [4.4% + 50.7%]) resulting in a $CD4^+/CD8^+$ ratio of 1.84 (Fig. 5B) was seen in PBMC recovered from an AK602-treated mouse, and the size of this $CD4^+$ cell population was comparable to that seen in a ddI-treated mouse (53.2% [3.8% + 49.4%]) and that in an uninfected mouse (48.9% [3.8% +

TABLE 1. Anti HIV-1 activity of novel SDP derivatives in PBMC[a]

Compound	IC_{50} value in p24 assay (nM)					
	HIV-1_{Ba-L} (R5)	HIV-1_{JRFL} (R5)	HIV-1_{MOKW} (R5)	HIV-1_{MM} ($R5_{MDR}$)	HIV-1_{JSL} ($R5_{MDR}$)	HIV-1_{NL4-3} (X4)
AK602	0.5 ± 0.3	0.2 ± 0.1	0.3 ± 0.2	0.7 ± 0.3	0.4 ± 0.2	>1,000
TAK779	14 ± 5	6 ± 2	9 ± 3	12 ± 4	10 ± 3	>1,000
SCH-C	3 ± 2	2 ± 1	2 ± 1.5	2.5 ± 1	2 ± 1	>1,000
ZDV	13 ± 5	7 ± 3	10 ± 6	520 ± 75	64 ± 13	9 ± 5
SQV	8 ± 3	6 ± 2	6 ± 3	212 ± 56	276 ± 44	10 ± 4

[a] IC_{50}s were determined by using PHA-PBMC isolated from three different donors, and the inhibition of p24 Gag protein production was used as an endpoint. All assays were conducted in triplicate. The results shown represent arithmetic means (±1 standard deviation) of three independently conducted assays. HIV-1_{MOKW} was isolated from a drug-naive AIDS patient, and HIV-1_{JSL} and HIV-1_{MM} were isolated from patients who received antiretroviral therapy for a long period of time and whose virus loads showed a number of RT and PR mutations. Two previously published CCR5 inhibitors, TAK779 and SCH-C, and zidovudine (ZDV) and saquinavar (SQV) were used as reference compounds.

45.1%]), resulting in the ratios of 1.43 and 1.40 (Fig. 5C and D), respectively. Figure 6A illustrates the overall profiles of $CD4^+/CD8^+$ cells ratios on day 16 in the four groups. The mean $CD4^+/CD8^+$ cell ratio in mice (n = 7) given saline was 0.1 (range, 0.06 to 0.20). In contrast, the ratios in AK602-treated mice (n = 8) were significantly higher with a mean value of 0.92 (range, 0.23 to 1.89; P = 0.001), which was comparable to that in ddI-treated mice (n = 9; mean, 1.29; range, 0.38 to 2.68; P = 0.001) and uninfected mice (n = 7; mean, 1.0; range, 0.50 to 1.49). The numbers of $CD4^+$ cells/μl

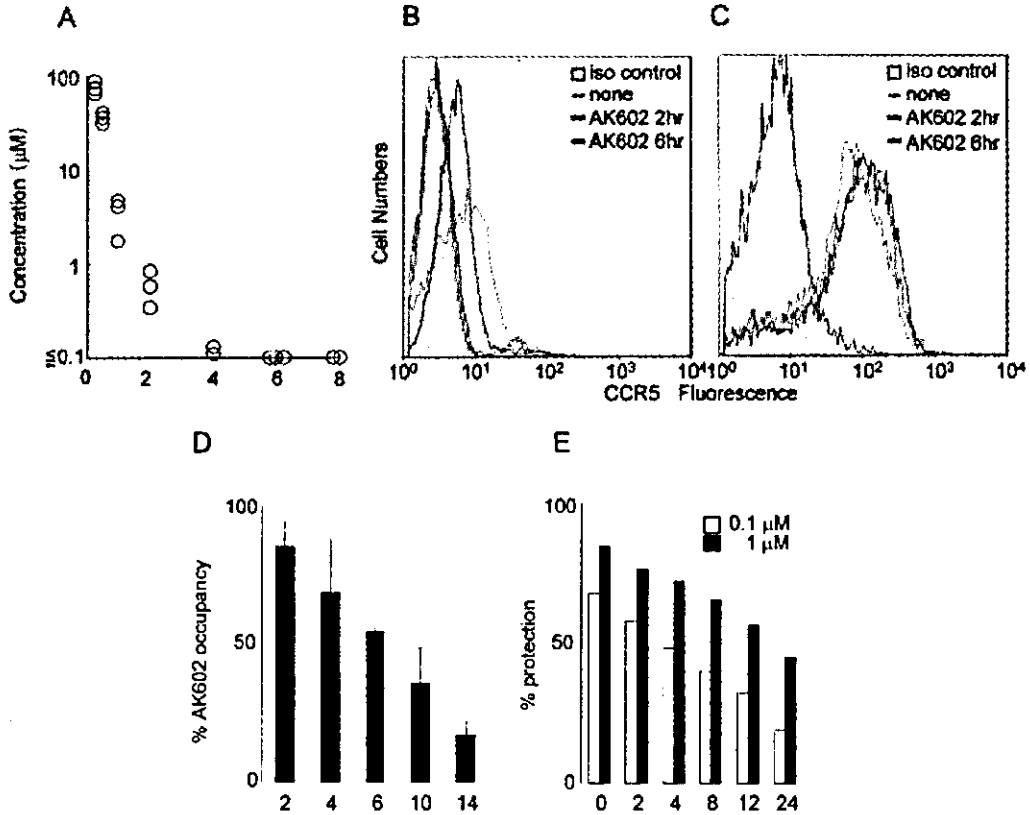

FIG. 4. Pharmacokinetics and persistence of anti-HIV-1 activity of AK602. (A) Pharmacokinetics of AK602. Each mouse was administered AK602 at a dose of 60 mg/kg, and blood samples were taken at 15, 30, 60, 120, 240, 480, and 720 min. Plasma concentrations of AK602 determined by HPLC analysis at 15, 30, 60, 120, and 240 min were 76.2, 36.1, 3.5, 0.6, and 0.13 μM, respectively. AK602 was not detected at later time points. (B and C) No CCR5 internalization or shedding was caused by AK602. Human PBMC were recovered 2 and 6 h after AK602 administration and stained with 45531 (B) or 3A9 (C). (D) Sustained AK602 occupancy on cell surfaces. At indicated periods of time after a bolus of AK-602 (60 mg/kg) was administered to hu-PBMC-NOG mice, PBMC were recovered and the percentages of AK602 occupancy on cellular CCR5 were determined with fluorescein isothiocyanate-conjugated monoclonal antibody 45531. (E) Persistence of in vitro activity of AK602 against R5 HIV-1 after AK602 depletion. $CCR5^+$ MAGI cells were exposed to 0.1 or 1 μM AK602 for 30 min and thoroughly washed to deplete AK602 from the medium. The cells were subsequently cultured for the indicated periods of time, exposed to HIV-1_{Ba-L}, and further cultured for 48 h, when the cells were harvested and lysed with Triton X-100-containing PBS. A solution containing chlorophenol red-β-D-galactopyranoside was added, the optical density was measured, and the percentage of protection was determined.

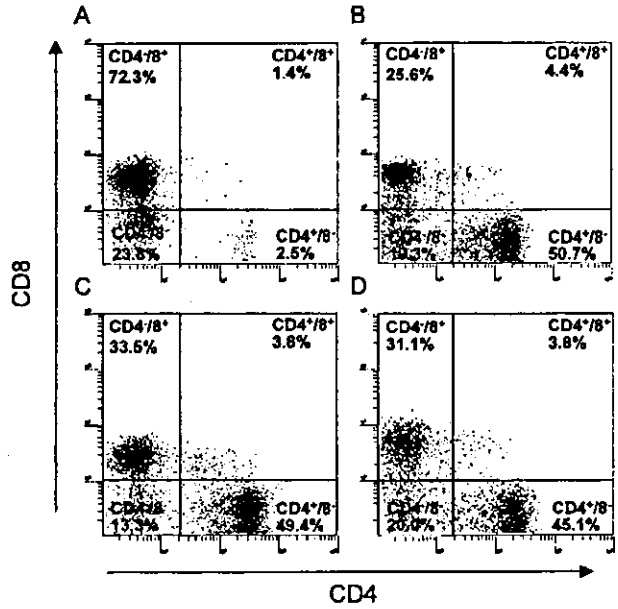

FIG. 5. Effects of AK602 on $CD4^+$ and $CD8^+$ cell counts in infected hu-PBMC-NOG mice. PBMC recovered on day 16 after R5 HIV-1 inoculation were subjected to flow cytometry. Shown are representative flow cytometric analysis profiles. Note that only 3.9% of $CD4^+$ cells were seen (A), resulting in a $CD4^+/CD8^+$ cell ratio of 0.05 in a mouse given saline, while distinct numbers of $CD4^+$ cells (55.1 and 53.2%) (B and C) were seen in AK602- and ddI-administered infected mice, resulting in $CD4^+/CD8^+$ cell ratios of 1.84 and 1.43, respectively. In an uninfected mouse (D), 48.9% of cells were positive for CD4, with a $CD4^+/CD8^+$ cell ratio of 1.40.

in saline-treated mice were significantly less than those of AK602-treated, ddI-treated, or uninfected mice (Fig. 6B).

Effects of AK602 on R5 HIV-1 proviral DNA copy numbers and serum p24 levels in R5 HIV-1-infected hu-PBMC-NOG mice. We next asked which population harbored proviral DNA in the cells recovered from R5 HIV-1-infected hu-PBMC-NOG mice, by purifying $CD4^+$ and $CD4^-$ cell populations and determining proviral DNA copy numbers in each population. As shown in Table 2, more than 99% of proviral DNA was found in $CD4^+$ cells and <0.3% of proviral DNA was detected in $CD4^-$ cells derived from saline-treated mice, indicating that R5 HIV-1 infection occurred in $CD4^+$ cells in the hu-PBMC-transplanted NOG environment. As illustrated in Fig. 6C, the mean number of R5 HIV-1 proviral DNA copies was 2.0×10^5 (range, 2.6×10^4 to 1.7×10^6) per 10^5 $CD4^+$ cells in R5 HIV-1-infected mice ($n = 7$) given saline. However, values for mice in groups given AK602 and ddI were 1.3×10^3 (range, 2.3×10^2 to 7.9×10^3; $P = 0.001$) and 1.8×10^2 (range, $<10^2$ to 7.9×10^2; $P = 0.001$), respectively.

The amounts of R5 HIV-1 p24 in serum were also found to be very high in saline-treated mice, with a mean amount of 1.1×10^5 pg/ml (range, 3.1×10^4 to 2.8×10^5 pg/ml). AK602 and ddI were found to significantly suppress the serum p24 amounts as examined on day 16 with a mean amount of 5.6×10^3 pg/ml (range, 8.1×10^2 to 2.1×10^4 pg/ml; $P = 0.001$) and 7.1×10^2 pg/ml (range, 1.3×10^2 to 1.1×10^4 pg/ml; $P = 0.001$), respectively (Fig. 6D).

AK602 suppressed R5 HIV-1 viremia in hu-PBMC-NOG mice. As described above, the PBMC transplanted to NOG mice were intensely activated in the xenogeneic environment and had undergone ~4 cycles of proliferation by day 2; a majority of the cells had undergone ≥10 cycles of proliferation by day 4 (Fig. 3B). These data suggested that R5 HIV-1 might extensively replicate in the hu-PBMC-NOG mice immediately after R5 HIV-1 inoculation. When we collected blood samples on days 5, 9, and 16 following the inoculation and determined R5 HIV-1 RNA copy numbers in infected, saline-treated mice ($n = 7$), the geometric mean copy number was 8.6×10^3/ml (range, 1.7×10^3 to 1.0×10^5) on day 5 and rapidly increased to 1.9×10^5/ml (range, 2.2×10^4 to 3.0×10^6) on day 9; by day 16, the mean copy number had reached 7.7×10^5/ml (range, 2.6×10^5 to 3.0×10^6/ml). However, AK602 significantly suppressed viremia by ~1.1 log, as examined on day 5; the mean numbers of R5 HIV-1 RNA copies in AK602-administered mice were 1.6 and 1.8 logs lower than those in saline-treated mice examined on days 9 and 16, respectively (Fig. 7). Comparable viremia suppression was seen in the mice receiving ddI (Fig. 7). It was noted that although AK602 did not completely prevent the viremia from further increasing after day 5, there was a clear reduction in the viremia increase rates. The mean slopes (change in RNA copies per day over the range of data from 5 to 16 days) for the group receiving saline was 0.167 ± 0.042, whereas those for the AK602 and ddI groups were 0.102 ± 0.041 and 0.091 ± 0.037, respectively. Thus, the rates of increase in the AK602 ($P = 0.0057$) and ddI ($P = 0.0023$) mice were significantly lower than that for the mice given saline, indicating that both of the agents significantly inhibited R5 HIV-1 replication in this mouse model over the range of days evaluated. No apparent AK602- or ddI-associated adverse effects were seen throughout the study period.

DISCUSSION

In the present hu-PBMC-NOG mouse model, human $CD4^+/CD8^+$ cell ratios went down to 0.1 by 16 days after R5 HIV-1 inoculation, the amounts of proviral DNA and p24 gag antigen reached 10^5 to 10^6 copies/10^5 $CD4^+$ cells and 10^5 pg/ml, respectively (Fig. 6), and no mice failed to be infected with R5 HIV-1. It is noteworthy that the use of NOG mice provides a higher engraftment rate than with other SCID mice such as NOD/Shi-SCID mice treated with anti-NK cell antibody or the β_2-microglobulin-deficient NOD-SCID mice (10). With NOG mice, the chimeric rate of 30 to 40% is achieved, and cord blood $CD34^+$ cells have been shown to "take" with as few as 100 cells (10). Moreover, all infected mice developed high levels of R5 HIV-1 viremia by day 16, reaching as high as 10^6 copies/ml (Fig. 7). It is worth noting that the notably high levels of HIV-1 viremia seen in the present mouse model by 16 days after R5 HIV-1 exposure can be seen only on acute infection or up to 10 years after HIV infection in humans (3, 4).

In the present study, we found that the conspicuous susceptibility to the infectivity and replication of R5 HIV-1 in these mice appeared to stem from the hyperactivation of the implanted human PBMC. The implanted PBMC were highly activated in the xenogeneic environment, expressed quite high

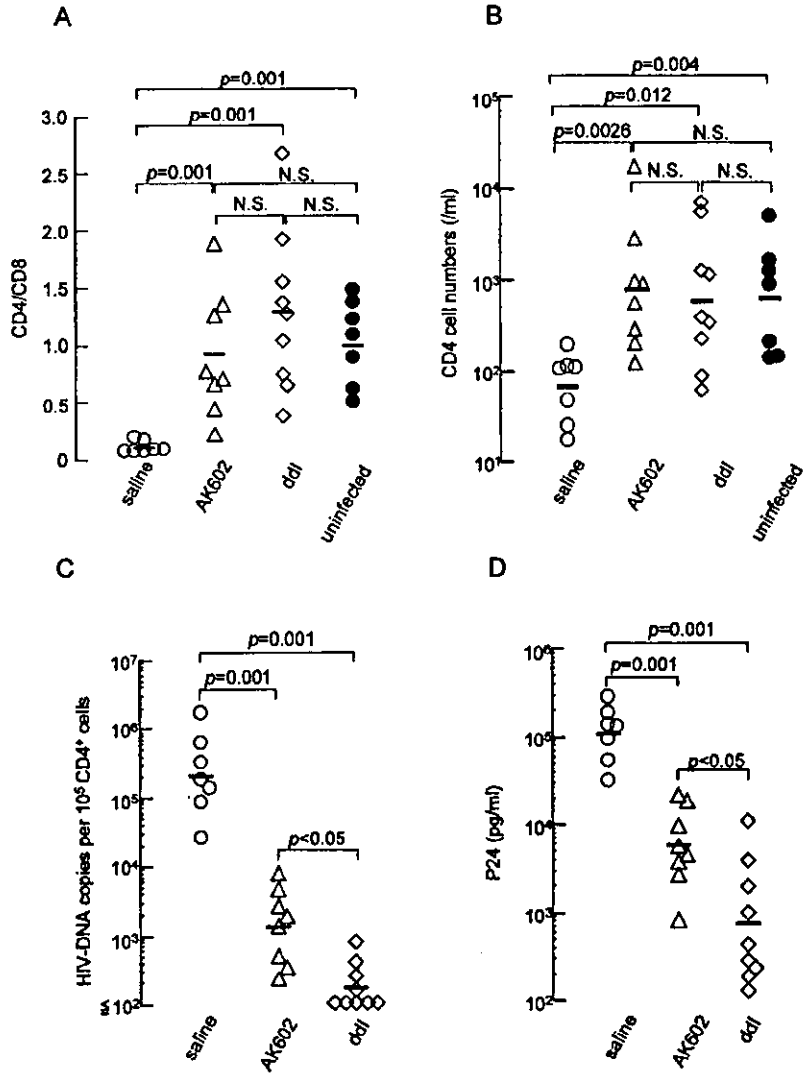

FIG. 6. Effects of AK602 on $CD4^+/CD8^+$ ratios and the amounts of proviral DNA and HIV-1 p24 in infected hu-PBMC-NOG mice. (A) Overall profiles of $CD4^+/CD8^+$ cell ratios. Note that the mean $CD4^+/CD8^+$ cell ratio in mice given saline (n = 7) was 0.1, while those in mice given AK602 or ddI were 0.92 and 1.29, respectively. The mean ratio in uninfected mice was 1.0. (B) Numbers of $CD4^+$ cells per microliter in each mouse group. (C) HIV-1 proviral DNA copy numbers in $CD4^+$ cells from each mouse group were determined by real-time PCR assay. Values are shown per 10^5 $CD4^+$ cells, as described in Materials and Methods. Note that the mean number of HIV-1 proviral DNA copies was 2.0×10^5 per 10^5 $CD4^+$ cells in mice given saline, while those in AK602- and ddI-treated groups were 1.3×10^3 and 1.8×10^2 per 10^5 $CD4^+$ cells (both, P = 0.001), respectively. (D) Amounts of plasma p24 antigen. Note that the amounts of p24 in plasma were high in saline-treated mice while AK602 and ddI significantly suppressed the serum p24 amounts as examined on day 16 after HIV-$1_{Ba\text{-}L}$ inoculation. The short bars indicate the arithmetic (A) and geometric (B, C, and D) means obtained.

levels of HLA-DR, and rapidly and continuously proliferated immediately after intraperitoneal infusion (Fig. 3A, B, and D). Moreover, the implanted PBMC expressed as much as 2.8-fold-higher levels of CCR5 on day 3 following implantation compared to PHA-PBMC on day 3 in culture (Fig. 3E). The combination of rapid proliferation and high levels of CCR5 expression of the implanted PBMC should explain the reason R5 HIV-1 rapidly replicated in the hu-PBMC-NOG mice and presented such high levels of R5 HIV-1 viremia. In this regard, only a few groups to date have documented the levels of viremia in the scientific literature. Among them are those by Garaci et al. (8) and Koyanagi et al. (14). The former documented high levels of viremia with a peak of 2.67×10^6 copies/ml in hu-PBL-NOD-SCID mice in which HIV-1-infected macrophages were inoculated, unlike our NOG mouse model where HIV-1 was directly inoculated. The latter report by Koyanagi et al. does not have viremia data but has data on p24 levels with a geometric mean of 11,092 pg/ml on day 14 after HIV-1 inoculation. However, the variation was much greater (178 to 1,434,444 pg/ml). Thus, one can say that the present model provides a greater reproducibility of high viremia levels than the mouse system reported by Koyanagi (14). It should be noted that the high levels of viremia and high engraftment rate achieved in this mouse model made it possible to monitor the

TABLE 2. Comparison of HIV-1 proviral DNA in human $CD4^+$ and $CD4^-$ cell fractions[a]

Sample	HIV-1 DNA copies (10^5 cells)		
	SCID-PBMC	$CD4^+$ cells	$CD4^-$ cells
Saline 1	138,858	162,193	461
Saline 2	135,967	117,949	<100
Saline 3	83,863	94,590	<100
AK602 1	3,390	2,300	<100
AK602 2	5,575	4,606	<100
AK602 3	1,925	1,398	<100
ddI 1	301	516	<100
ddI 2	793	1,317	<100
ddI 3	<100	118	<100

[a] HIV-1 proviral DNA copy numbers were determined by real-time PCR assay of unseparated human PBMC and purified $CD4^+$ and $CD4^-$ cells, following recovery from hu-PBMC-NOG mice. Values are shown per 10^5 cells, as described in Materials and Methods.

changes in the viremia levels periodically in the same set of mice without sacrificing them, while most of the previously described SCID mouse models required mice to be sacrificed at each time point of testing (25, 29, 30) or needed further in vitro coculture of the PBMC recovered from the mice with freshly prepared uninfected target cells for an additional period of days (9, 34).

We demonstrated in this study that a novel SDP derivative, AK602, exerted highly potent activity against laboratory and primary R5 HIV-1 strains as well as MDR R5 HIV-1 variant with IC_{50} values of subnanomolar concentrations (Table 1). It should be noted that AK602 represents a novel SDP derivative, which binds to human CCR5 but not to human CXCR4, CCR1, CCR2, CCR3, CCR4 or murine CCR5; blocks the binding of MIP-1α to CCR5 with an extremely high affinity (K_d values of ~3 nM); potently blocks HIV-1-gp120/CCR5 binding; and exerts potent activity against a wide spectrum of laboratory and primary R5 HIV-1 isolates including MDR HIV-1 and HIV-1 strains of various clades with IC_{50} values of 0.2 to 0.6 nM in vitro (K. Maeda, H. Ogata, S. Harada, Y. Tojo, T. Miyakawa, H. Nakata, Y. Takaoka, S. Shibayama, D. Fukushima, J. Moravek, E. Arnold, and H. Mitsuya, 11th Conf. Retrovir. Opp. Infect., abstr. 540, 2004; J. Demarest et al., XV Int. AIDS Conf., abstr. WeOrA1231, 2004). The plasma half-life of AK602 in the hu-PBMC-NOG mice, however, proved to be as short as 29 min when the agent was administered intraperitoneally (Fig. 4A). Considering that AK602 possesses such a high binding affinity to CCR5, we presumed that AK602 could remain on CCR5 for an extended period of time even after the agent was removed from the bloodstream in mice. The high and extensive level of AK602 occupancy observed in PBMC recovered from mice receiving AK602 substantiated this presumption (Fig. 4D). The subsequent in vitro experiment in which $CCR5^+$ MAGI cells were incubated with AK602 but exposed to R5 HIV-1 after the removal of the compound from the culture medium showed that AK602's anti-R5 HIV-1 activity can persist for an extensive period of time even if AK602 is no longer present in the culture (Fig. 4E). It is of note that unlike certain reports of in vivo anti-HIV-1 activity of chemokine antagonists which were administered before HIV-1 inoculation, thus demonstrating prophylactic effects of such agents (9, 30), the present system demonstrates anti-HIV-1 treatment after the establishment of HIV-1 infection, analogous to antiviral therapy in clinical settings.

When highly active antiretroviral therapy exerts its potent antiviral effects in clinical settings, a decrease in HIV-1 viremia is seen often within weeks, ultimately resulting in undetectable viremia; however in the present study, the viremia levels in mice receiving AK602 or ddI continued to increase although the rate of increment significantly declined (Fig. 7). The failure of AK602 and ddI to decrease viremia levels could be due in part to such a rapid viral replication in hyperactivated and proliferating $CD4^+$ cells. As discussed earlier, PBMC recovered from the hu-PBMC-NOG mice were highly positive for CCR5 and HLA-DR (Fig. 3D and E), compared to the levels of activation seen in the same donor's PHA-PBMC. It should be noted, however, that the mean numbers of proviral DNA copies on day 16 in mice receiving AK602 and ddI were 1.3×10^3 and 1.8×10^2 per 10^5 $CD4^+$ cells, respectively (Fig. 6C), suggesting that most $CD4^+$ cells (98.7 and 99.8% on average, respectively) were free of HIV-1 and proliferating in those

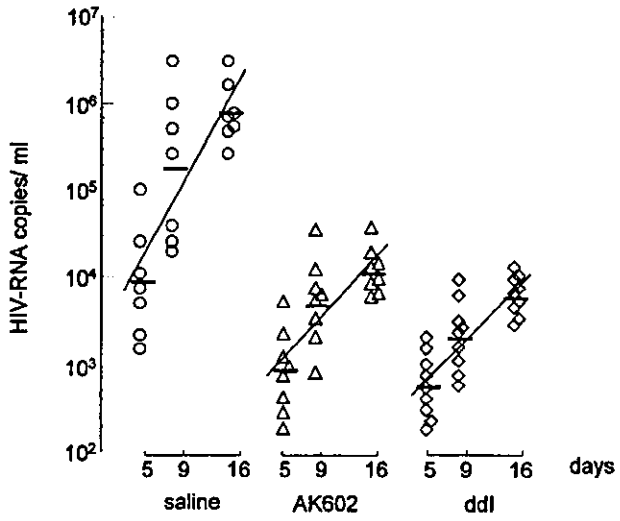

FIG. 7. AK602 suppresses R5 HIV-1 viremia in hu-PBMC-NOG mice. Blood samples were collected on days 5, 9, and 16 after inoculation and were subjected to the determination of R5 HIV-1 RNA copy numbers. Note that the copy numbers in saline-treated mice rapidly increased and reached ~10^6/ml by day 16, while AK602 significantly suppressed the viremia by 1.6 and 1.8 logs as examined on day 9 ($P = 0.001$ compared to saline-treated mice) and day 16 ($P = 0.001$), respectively. Comparable viremia suppression was seen in ddI-treated mice, except on day 16, when ddI activity was greater than that of AK602 ($P = 0.027$). Note that there was a clear reduction in the rate of increase of viremia as well. When the values of $\log_{10}$ HIV-1 RNA copies were calculated and the slopes corresponding to the rates of increase per day were determined, the resulting mean slope (solid line) for the saline-treated mice was 0.167 ± 0.042, whereas those for the AK602- and ddI-treated mice were 0.102 ± 0.041 and 0.091 ± 0.037, respectively. The increase rate for saline-treated mice was significantly higher than those of AK602-treated mice ($P = 0.0057$) and ddI-treated mice ($P = 0.0023$), respectively. The horizontal bars and solid lines represent the geometric means of HIV-1 RNA copy numbers and the slopes calculated, respectively.

mice on day 16 after the virus inoculation, if one copy of proviral DNA was postulated to reside in one $CD4^+$ cell.

One of us (Y.K.) previously attempted to investigate the mechanism of $CD4^+$ cell depletion seen in individuals with HIV-1 infection by employing a PBMC-transplanted NOD (NOD/Shi) *scid/scid* mouse system (24). Massive apoptosis was observed in HIV-1-uninfected $CD4^+$ cells in the spleens of the HIV-1-infected NOD-*scid/scid* mice. A combination of terminal deoxynucleotidyl transferase-mediated dUTP nick-end labeling and immunostaining for death-inducing tumor necrosis factor (TNF) family molecules showed that apoptotic cells were frequently found in conjugation with TNF-related apoptosis-inducing ligand (TRAIL)-expressing $CD3^+$ $CD4^+$ human T cells. Further observation that a neutralizing anti-TRAIL antibody inhibited the development of $CD4^+$ cell apoptosis suggested that a large number of HIV-1-uninfected $CD4^+$ cells undergo TRAIL-mediated apoptosis, contributing to the marked depletion of $CD4^+$ cells (24). The observation by Miura and his colleagues that the number of TRAIL-positive cells was consistently higher in HIV-1-infected mice than in uninfected ones makes it apparent that TRAIL expression is induced upon HIV-1 infection (23, 24). In this regard, the present observation that AK602 and ddI potently blocked the decrease in $CD4^+$ cells in spite of the rather increasing HIV-1 viremia in the face of AK602 or ddI (Fig. 7) suggests that the mere presence of viremia might not be sufficient for the HIV-induced apoptosis in $CD4^+$ cells. Our observation that most surviving $CD4^+$ cells in mice receiving AK602 or ddI were free of HIV-1 (see above) suggests that these anti-HIV-1 agents might block not only de novo HIV-1 infection, but also bystander killing of uninfected $CD4^+$ cells. The present data also suggest that a certain factor(s) such as cytokines produced by the freshly HIV-1-infected cells might mediate the apoptosis of bystander $CD4^+$ cells through the upregulation of TRAIL expression, death receptors (e.g., DR4 and DR5), and/or downregulation of decoy receptors (e.g., DcR1 and DcR2) (26, 27). However, experiments with a combination of terminal deoxynucleotidyl transferase-mediated dUTP nick-end labeling and TNF family molecules have to be conducted for better understanding of the bystander killing in regard to AK602's effects.

It is of note that several CCR5 antagonists are currently in various stages of development. AK602 has recently been administered to healthy adult subjects in a phase I clinical trial and shown to bind to CCR5 for an extended period of time, suggesting that an oral formulation with fewer administrations and lower dosage is possible for AK602 as a therapeutic agent for HIV-1 infection (J. Demarest, K. Adkison, S. Sparks, A. Shachoy-Clark, K. Schell, S. Reddy, L. Fang, K. O'Mara, S. Shibayama, and S. Piscitelli, 11th Conf. Retrovir. Opp. Infect., abstr. 139, 2004). Taken together, our observations that plasma viral load reached $\sim 10^6$ RNA copies/ml and that AK602 potently inhibited the replication of R5 HIV-1 strongly suggest that the present hu-PBMC-NOG mouse AIDS model could serve as a useful instrument for analyzing the pathogenesis of HIV-1 infection and testing the efficacy of antiviral agents.

ACKNOWLEDGMENTS

We thank Seth Steinberg for statistical analysis and Naoko Misawa, Yuji Kawano, and Hiromi Ogata for technical assistance and discussion.

This work was supported in part by grant-in-aids for Scientific Research on Priority Areas (14207025 and 15019086) from the Japanese Ministry of Education, Science, Sports, Culture and Technology of Japan (Monbu-Kagakusho) and a grant for AIDS Research (H15-AIDS-001) from the Ministry of Health, Labor, and Welfare of Japan (Kosei-Rohdosho).

REFERENCES

1. **Baba, M., O. Nishimura, N. Kanzaki, M. Okamoto, H. Sawada, Y. Iizawa, M. Shiraishi, Y. Aramaki, K. Okonogi, Y. Ogawa, K. Meguro, and M. Fujino.** 1999. A small-molecule, nonpeptide CCR5 antagonist with highly potent and selective anti HIV-1 activity. Proc. Natl. Acad. Sci. USA 96:5698–5703.
2. **Carr, A., K. Samaras, A. Thorisdottir, G. R. Kaufmann, D. J. Chisholm, and D. A. Cooper.** 1999. Diagnosis, prediction, and natural course of HIV-1 protease-inhibitor associated lipodystrophy, hyperlipidaemia, and diabetes mellitus: a cohort study. Lancet 353:2093–2099.
3. **Dean, M., M. Carrington, C. Winkler, G. A. Huttley, M. W. Smith, R. Allikmets, J. J. Goedert, S. P. Buchbinder, E. Vittinghoff, E. Gomperts, S. Donfield, D. Vlahov, R. Kaslow, A. Saah, C. Rinaldo, R. Detels, and S. J. O'Brien.** 1996. Genetic restriction of HIV-1 infection and progression to AIDS by a deletion allele of the CKR5 structural gene. Hemophilia Growth and Development Study, Multicenter AIDS Cohort Study, Multicenter Hemophilia Cohort Study, San Francisco City Cohort, ALIVE Study. Science 273:1856–1862.
4. **Easterbrook, P. J.** 1999. Long-term non-progression in HIV infection: definitions and epidemiological issues. J. Infect. 38:71–73.
5. **Fauci, A. S.** 1999. The AIDS epidemic—considerations for the 21st century. N. Engl. J. Med. 341:1046–1050.
6. **Finzi, D., J. Blankson, J. D. Siliciano, J. B. Margolick, K. Chadwick, T. Pierson, K. Smith, J. Lisziewicz, F. Lori, C. Flexner, T. C. Quinn, R. E. Chaisson, E. Rosenberg, B. Walker, S. Gange, J. Gallant, and R. F. Siliciano.** 1999. Latent infection of CD4+ T cells provides a mechanism for lifelong persistence of HIV-1, even in patients on effective combination therapy. Nat. Med. 5:512–517.
7. **Gartner, S., P. Markovits, D. M. Markovitz, M. H. Kaplan, R. C. Gallo, and M. Popovic.** 1986. The role of mononuclear phagocytes in HTLV-III/LAV infection. Science 233:215–219.
8. **Garaci, E., S. Aquaro, C. Lapenta, A. Amendola, M. Spada, S. Covaceuszach, C. F. Perno, and F. Belardelli.** 2003. Anti-nerve growth factor Ab abrogates macrophage-mediated HIV-1 infection and depletion of CD4+ T lymphocytes in hu-SCID mice. Proc. Natl. Acad. Sci. USA 100:8927–8932.
9. **Ichiyama, K., S. Yokoyama-Kumakura, Y. Tanaka, R. Tanaka, K. Hirose, K. Bannai, T. Edamatsu, M. Yanaka, Y. Niitani, N. Miyano-Kurosaki, H. Takaku, Y. Koyanagi, and N. Yamamoto.** 2003. A duodenally absorbable CXC chemokine receptor 4 antagonist, KRH-1636, exhibits a potent and selective anti-HIV-1 activity. Proc. Natl. Acad. Sci. USA 100:4185–4190.
10. **Ito, M., H. Hiramatsu, K. Kobayashi, K. Suzue, M. Kawahata, K. Hioki, Y. Ueyama, Y. Koyanagi, K. Sugamura, K. Tsuji, T. Heike, and T. Nakahata.** 2002. NOD/SCID/γ(c)(null) mouse: an excellent recipient mouse model for engraftment of human cells. Blood 100:3175–3182.
11. **Kavlick, M. F., and H. Mitsuya.** 2001. The emergence of drug resistant HIV-1 variants and its impact on antiretroviral therapy of HIV-1 infection, p. 279–312. *In* E. De Clercq (ed.), The art of antiretroviral therapy. American Society for Microbiology, Washington, D.C.
12. **Koh, Y., H. Nakata, K. Maeda, H. Ogata, G. Bilcer, T. Devasamudram, J. F. Kincaid, P. Boross, Y. F. Wang, Y. Tie, P. Volarath, L. Gaddis, R. W. Harrison, I. T. Weber, A. K. Ghosh, and H. Mitsuya.** 2003. Novel bis-tetrahydrofuranylurethane-containing nonpeptidic protease inhibitor (PI) UIC-94017 (TMC114) with potent activity against multi-PI-resistant human immunodeficiency virus in vitro. Antimicrob. Agents Chemother. 47:3123–3129.
13. **Koyanagi, Y., S. Miles, R. T. Mitsuyasu, J. E. Merrill, H. V. Vinters, and I. S. Chen.** 1987. Dual infection of the central nervous system by AIDS viruses with distinct cellular tropisms. Science 236:819–822.
14. **Koyanagi, Y., Y. Tanaka, J. Kira, M. Ito, K. Hioki, N. Misawa, Y. Kawano, K. Yamasaki, R. Tanaka, Y. Suzuki, Y. Ueyama, E. Terada, T. Tanaka, M. Miyasaka, T. Kobayashi, Y. Kumazawa, and N. Yamamoto.** 1997. Primary human immunodeficiency virus type 1 viremia and central nervous system invasion in a novel hu-PBL-immunodeficient mouse strain. J. Virol. 71:2417–2424.
15. **Lee, B., M. Sharron, L. J. Montaner, D. Weissman, and R. W. Doms.** 1999. Quantification of CD4, CCR5, and CXCR4 levels on lymphocyte subsets, dendritic cells, and differentially conditioned monocyte-derived macrophages. Proc. Natl. Acad. Sci. USA 96:5215–5220.
16. **Lyons, A. B.** 2000. Analysing cell division in vivo and in vitro using flow cytometric measurement of CFSE dye dilution. J. Immunol. Methods 243: 147–154.
17. **Maeda, K., K. Yoshimura, S. Shibayama, H. Habashita, H. Tada, K. Sagawa, T. Miyakawa, M. Aoki, D. Fukushima, and H. Mitsuya.** 2001. Novel low molecular weight spirodiketopiperazine derivatives potently inhibit R5

HIV-1 infection through their antagonistic effects on CCR5. J. Biol. Chem. 276:35194–35200.
18. **Maeda, Y., M. Foda, S. Matsushita, and S. Harada.** 2000. Involvement of both the V2 and V3 regions of the CCR5-tropic human immunodeficiency virus type 1 envelope in reduced sensitivity to macrophage inflammatory protein 1α. J. Virol. 74:1787–1793.
19. **McCune, J. M., R. Namikawa, C. C. Shih, L. Rabin, and H. Kaneshima.** 1990. Suppression of HIV infection in AZT-treated SCID-hu mice. Science 247:564–566.
20. **Mitsuya, H., and S. Broder.** 1986. Inhibition of the in vitro infectivity and cytopathic effect of human T-lymphotropic virus type III/lymphadenopathy virus-associated virus (HTLV-III/LAV) by 2′,3′-dideoxynucleosides. Proc. Natl. Acad. Sci. USA 83:1911–1915.
21. **Mitsuya, H., and S. Broder.** 1987. Strategies for antiviral therapy in AIDS. Nature 325:773–778.
22. **Mitsuya, H., and J. Erickson.** 1999. Discovery and development of antiretroviral therapeutics for HIV infection, p. 751–780. *In* T. C. Merigan, J. G. Bartlet, and D. Bolognesi (ed.). Textbook of AIDS medicine. Williams & Wilkins, Baltimore, Md.
23. **Miura, Y., N. Misawa, Y. Kawano, H. Okada, Y. Inagaki, N. Yamamoto, M. Ito, H. Yagita, K. Okumura, H. Mizusawa, and Y. Koyanagi.** 2003. Tumor necrosis factor-related apoptosis-inducing ligand induces neuronal death in a murine model of HIV central nervous system infection. Proc. Natl. Acad. Sci. USA 100:2777–2782.
24. **Miura, Y., N. Misawa, N. Maeda, Y. Inagaki, Y. Tanaka, M. Ito, N. Kayagaki, N. Yamamoto, H. Yagita, H. Mizusawa, and Y. Koyanagi.** 2001. Critical contribution of tumor necrosis factor-related apoptosis-inducing ligand (TRAIL) to apoptosis of human CD4+ T cells in HIV-1-infected hu-PBL-NOD-SCID mice. J. Exp. Med. 193:651–660.
25. **Mosier, D. E., R. J. Gulizia, S. M. Baird, D. B. Wilson, D. H. Spector, and S. A. Spector.** 1991. Human immunodeficiency virus infection of human-PBL-SCID mice. Science 251:791–794.
26. **Pan, G., J. Ni, Y. F. Wei, G. Yu, R. Gentz, and V. M. Dixit.** 1997. An antagonist decoy receptor and a death domain-containing receptor for TRAIL. Science 277:815–818.
27. **Pan, G., K. O'Rourke, A. M. Chinnaiyan, R. Gentz, R. Ebner, J. Ni, and V. M. Dixit.** 1997. The receptor for the cytotoxic ligand TRAIL. Science 276:111–113.
28. **Ratain, M., and W. Plunkett.** 1997. Pharmacology, p. 875–889. *In* J. Holland, R. Bast, Jr., D. Morton, E. Frei, D. KuFe, and R. Weichselbaum (ed.), Cancer medicine, 4th ed. Williams and Wilkins, Baltimore, Md.
29. **Ruxrungtham, K., E. Boone, H. Ford, Jr., J. S. Driscoll, R. T. Davey, Jr., and H. C. Lane.** 1996. Potent activity of 2′-β-fluoro-2′,3′-dideoxyadenosine against human immunodeficiency virus type 1 infection in hu-PBL-SCID mice. Antimicrob. Agents Chemother. 40:2369–2374.
30. **Strizki, J. M., S. Xu, N. E. Wagner, L. Wojcik, J. Liu, Y. Hou, M. Endres, A. Palani, S. Shapiro, J. W. Clader, W. J. Greenlee, J. R. Tagat, S. McCombie, K. Cox, A. B. Fawzi, C. C. Chou, C. Pugliese-Sivo, L. Davies, M. E. Moreno, D. D. Ho, A. Trkola, C. A. Stoddart, J. P. Moore, G. R. Reyes, and B. M. Baroudy.** 2001. SCH-C (SCH 351125), an orally bioavailable, small molecule antagonist of the chemokine receptor CCR5, is a potent inhibitor of HIV-1 infection in vitro and in vivo. Proc. Natl. Acad. Sci. USA 98:12718–12723.
31. **Walker, U. A., B. Setzer, and N. Venhoff.** 2002. Increased long-term mitochondrial toxicity in combinations of nucleoside analogue reverse-transcriptase inhibitors. AIDS 16:2165–2173.
32. **Westervelt, P., H. E. Gendelman, and L. Ratner.** 1991. Identification of a determinant within the human immunodeficiency virus 1 surface envelope glycoprotein critical for productive infection of primary monocytes. Proc. Natl. Acad. Sci. USA 88:3097–3101.
33. **Yahata, T., K. Ando, Y. Nakamura, Y. Ueyama, K. Shimamura, N. Tamaoki, S. Kato, and T. Hotta.** 2002. Functional human T lymphocyte development from cord blood CD34+ cells in nonobese diabetic/Shi-scid, IL-2 receptor gamma null mice. J. Immunol. 169:204–209.
34. **Yoshida, A., R. Tanaka, T. Murakami, Y. Takahashi, Y. Koyanagi, M. Nakamura, M. Ito, N. Yamamoto, and Y. Tanaka.** 2003. Induction of protective immune responses against R5 human immunodeficiency virus type 1 (HIV-1) infection in hu-PBL-SCID mice by intrasplenic immunization with HIV-1-pulsed dendritic cells: possible involvement of a novel factor of human CD4(+) T-cell origin. J. Virol. 77:8719–8728.
35. **Yoshimura, K., R. Kato, K. Yusa, M. F. Kavlick, V. Maroun, A. Nguyen, T. Mimoto, T. Ueno, M. Shintani, J. Falloon, H. Masur, H. Hayashi, J. Erickson, and H. Mitsuya.** 1999. JE-2147: a dipeptide protease inhibitor (PI) that potently inhibits multi-PI-resistant HIV-1. Proc. Natl. Acad. Sci. USA 96: 8675–8680.

ELSEVIER

Journal of Neuroimmunology 151 (2004) 189–194

Journal of Neuroimmunology

www.elsevier.com/locate/jneuroim

Short communication

Th1/Th2 balance and HTLV-I proviral load in HAM/TSP patients treated with interferon-α

Juan Feng[a], Tatsuro Misu[a], Kazuo Fujihara[a,*], Naoko Misawa[b], Yoshio Koyanagi[b], Yusei Shiga[a], Atsushi Takeda[a], Shigeru Sato[c], Sadao Takase[c], Takeshi Kohnosu[d], Hiroshi Saito[d], Yasuto Itoyama[a]

[a] *Department of Neurology, Tohoku University School of Medicine 1-1 Seiryomachi, Aobaku, Sendai 980-8574, Japan*
[b] *Department of Microbiology, Tohoku University School of Medicine, Japan*
[c] *Department of Neurology, Kohnan Hospital, Japan*
[d] *Department of Neurology, National Nishitaga Hospital, Japan*

Received 6 October 2003; received in revised form 15 January 2004; accepted 20 February 2004

Abstract

We studied the immunological and virological effects of interferon-α (IFN-α) therapy in nine patients with HTLV-I-associated myelopathy (HAM/TSP). After therapy, the percentages of CCR5+ cells in CD4+ cells significantly decreased in the cerebrospinal fluid as well as blood. The therapy also significantly lowered the intracellular IFN-γ+/interleukin-4+ T-cell ratio in blood. Those helper T-cell type 1 (Th1)-related responses tended to be higher and reduce more evidently following therapy in three patients who clinically improved. Also, all the three patients had one or more HTLV-I copies in five blood mononuclear cells. These results suggest that IFN-α suppresses Th1 responses in HAM/TSP and that the patients with higher Th1 immunity and proviral loads may be responders of the therapy. Larger-scale studies are needed to confirm the findings.

Keywords: HAM/TSP; HTLV-I; Interferon-alpha therapy; Helper T cell; Chemokine receptor

1. Introduction

Human T-lymphotropic virus type I (HTLV-I) is associated with chronic inflammatory myelopathy, HTLV-I-associated myelopathy/tropical spastic paraparesis (HAM/TSP) (Gessain et al., 1985; Osame et al., 1986; Izumo et al., 2000). Previous studies demonstrated remarkable immune activation including helper T-cell type 1 (Th1)-associated responses (Kuroda and Matsui, 1993; Itoyama et al., 1996; Umehara et al., 1994; Jacobson et al., 1998) and high HTLV-I proviral loads (Nagai et al., 1998) in HAM/TSP. These immunological and virological changes are probably important in the pathogenesis of this myelopathy and effective immunotherapies for HAM/TSP need to suppress these abnormalities.

A randomized, double-blind study demonstrated that interferon-α (IFN-α) was clinically effective in HAM/TSP (Izumo et al., 1996). The immunological effects of the therapy had been unclear, but we recently found a significant reduction of CD4 cell subsets in the cerebrospinal fluid (CSF) of the patients receiving the therapy (Feng et al., 2003). Here, we report Th1 and Th2-associated chemokine receptor expression on T cells, intracellular cytokine levels in T cells and HTLV-I proviral loads in blood before and after the therapy in the same patients.

2. Materials and methods

2.1. Subjects

Nine patients (five women and four men) were enrolled in the present study as reported previously (Feng et al., 2003). Their ages ranged from 54 to 72 years old and the duration of disease was from 2 to 50 years. The clinical disability was graded according to the Osame's scale: motor

* Corresponding author. Tel.: +81-22-717-7189; fax: +81-22-717-7192.
E-mail address: fujikazu@em.neurol.med.tohoku.ac.jp (K. Fujihara).

0165-5728/$ - see front matter © 2004 Elsevier B.V. All rights reserved.
doi:10.1016/j.jneuroim.2004.02.007

disability: grade 0 (normal)–13 (bedridden), dysuria: grade 0 (normal)–3 (severe) (Izumo et al., 1996). The patients received intramuscular injections of IFN-α (3 million units) daily for 4 weeks (Izumo et al., 1996). None had received immunosuppressants for the last 3 months except for a single patient (HAM3) who was treated with a fixed dose of oral prednisolone (20 mg/day) throughout the therapy. Age- and sex-matched nine HTLV-I-seronegative control subjects were studied for peripheral blood mononuclear cells (PBMC). We obtained informed consents prior to the study and the present study conformed to the guidelines of Medical Ethics Committee of our medical school.

2.2. Mononuclear cell preparation

Heparinized venous blood and CSF were collected before the IFN-α therapy and the next day of the last IFN-α injection. PBMC were isolated by Ficoll-Paque and CSF cells were directly isolated by centrifugation.

2.3. Flow cytometric analysis

2.3.1. T-cell subset

We analyzed T-cell subsets using a standard direct immunofluorescent technique with monoclonal antibodies (MoAbs), a three-color flow cytometer (FACSCalibur, Becton Dickinson, San Jose, CA) and the CellQuest software.

The analyzed subsets were CCR5+ and CXCR3+ (helper T-cell type 1 [Th1]-associated chemokine receptor expressing cells) and CCR3+ (Th2-associated chemokine receptor expressing cells, especially in the early stage of Th2 response) among CD4+ and CD8+ cells. Peridinin chlorophyll protein-conjugated anti-CD4 and anti-CD8, fluorescein isothiocyanate-conjugated anti-CD8 MoAbs were provided by Becton Dickinson. Phycoerythrin-conjugated anti-CCR5 and anti-CCR3 and carboxy-fluorescein succinimidylester-conjugated anti-CXCR3 MoAbs were purchased from Dako (Tokyo, Japan).

The data were expressed as the percentages of T-cell subsets in CD4+ or CD8+ cells.

2.3.2. Intracellular Th1/Th2-associated cytokines

The ratio of IFN-γ producing cells to interleukin-4 (IL-4) producing cells in CD3+ cells was assayed with a FACSCalibur according to the previous report (Pala et al., 2000).

2.4. HTLV-I proviral load in PBMC

DNA was extracted from PBMC. The HTLV-I proviral load was quantified using a real-time Taq-Man PCR method (PE Applied Biosystems, Foster City, CA). Standard curves of β-actin and HTLV-I tax genes were generated using DNA derived from an HTLV-I infected cell line, TloM1. TaqMan amplifications were carried out with the forward primers 5′-ACTCCTCAAGCGAGCTGCAT-3′, the reverse primer 5′-TTTTTCTTTGGGATCGGCG-3′ (Greiner Japan, Tokyo, Japan) and HTLV-I TaqMan Probe 5′-CCCAAGACCC-GTCGGAGGCC-3′ labeled with the 5′ FAM reporter dye and the 3′ TAMRA quencher dye molecules (Japan BioService, Asaka, Japan). The primers and probe for β-actin gene were obtained from PE Applied Biosystems. The thermal cycle conditions were 50 °C for 2 min followed by 95 °C for 10 min (hot start) and then 40 cycles were run by melting at 95 °C for 15 s and annealing/extension at 60 °C for 1 min in each cycle. Each sample was analyzed in triplicate. For each reaction, 100 ng of DNA, the equivalent of 2×10^4 cells, were subjected to the analysis. The amplifications were performed on an ABI PRISM 7700 sequence detector equipped with a 96-well thermal cycler. Copy numbers were reported as copy equivalents per 10^5 PBMC.

2.5. Statistical analysis

We used Mann–Whitney *U*-test to compare the unpaired values, Wilcoxon's signed rank test to compare the paired values. We also examined correlations in clinical disability, immunological and virological parameters (motor disability grade, percentages of CCR5+, CXCR3+ and CCR3+ in CD4+ cells, and CCR5+, CXCR3+ and CCR3+ in CD8+ cells in the CSF and blood, ratio of IFN-γ producing cells to IL-4 producing cells in blood CD3+ cells, and HTLV-I proviral load) of the HAM/TSP patients with Spearman rank correlation coefficient test. Correlations in both baseline values and the changes after the IFN-α therapy were analyzed. *P*-values less than 0.05 were considered statistically significant.

3. Results

3.1. Clinical effects

The motor disability grade improved in three patients after the IFN-α therapy (Patients HAM 3, grade 3 → 2; HAM 5, grade 8 → 6; HAM 6, grade 6 → 4) as we reported (Feng et al., 2003). The dysuria grade did not change.

3.2. T-cell subsets (Table 1)

3.2.1. CCR5

The percentage of CCR5+ cells in blood CD4+ cells was significantly higher before the IFN-α therapy in HAM/TSP than in control. In HAM/TSP, the mean percentages of all CCR5+ T-cell subsets in blood and CSF decreased after the therapy. Among them, the percentage of CCR5+ cells in blood CD4+ cells of HAM/TSP significantly decreased after the therapy, and they were no longer different between HSM/TSP and control. The percentage of CCR5+ cells in CSF CD4+ cells also significantly decreased after the therapy (Table 1).

Table 1
T cells expressing Th1/Th2-associated chemokine receptors in HAM/TSP patients treated with interferon-α and in control subjects

	CCR5+ in CD4+	CXCR3+ in CD4+	CCR3+ in CD4+
Control (n=9)	(%)	(%)	(%)
Blood	0.5 ± 0.1	27.3 ± 4.8	0.3 ± 0.1
HAM/TSP (n=9)			
Blood			
before IFN-α	1.5 ± 0.9 *	27.9 ± 12.3	0.3 ± 0.2
after IFN-α	0.9 ± 0.8 *	25.5 ± 7.6	0.4 ± 0.2
CSF			
before IFN-α	20.5 ± 8.8 *	88.5 ± 5.4	4.3 ± 4.3
after IFN-α	13.4 ± 5.3 *	81.3 ± 12.2	7.5 ± 3.1
	CCR5+ in CD8+	CXCR3+ in CD8+	CCR3+ in CD8+
Control (n=9)	(%)	(%)	(%)
Blood	0.9 ± 0.9	35.9 ± 8.1	0.5 ± 0.2
HAM/TSP (n=9)			
Blood		*	
before IFN-α	3.0 ± 4.5	55.5 ± 17.4	0.7 ± 0.4
after IFN-α	1.6 ± 1.0	36.4 ± 17.6 *	0.6 ± 0.2
CSF			
before IFN-α	27.1 ± 12.1	94.8 ± 4.4	4.3 ± 4.3
after IFN-α	17.9 ± 6.5	90.3 ± 9.3	7.5 ± 3.6

Data are mean percentages ± standard deviation.
*$P < 0.05$.

The percentage of CCR5+ cells in CSF CD4 cells was unequivocally higher in the three patients who clinically improved after the therapy (the lowest value was 26.8% in Patient HAM 6) than in the six patients without clinical effect (the highest value was 18.3% in Patient HAM 2).

3.2.2. CXCR3

In blood, the percentages of CXCR3+ cells in CD8+ cells were significantly higher in HAM/TSP before the therapy than in control. In HAM/TSP, the mean percentages of all CXCR3+ T-cell subsets in blood and CSF decreased after the therapy. Among them, the percentage of CXCR3+ cells in CD8+ cells significantly decreased after the therapy in HAM/TSP, and it was no longer different between HAM/TSP and control.

3.2.3. CCR3

No CCR3+ subset was significantly different between HAM/TSP and control or changed significantly after the therapy in HAM/TSP, although the mean percentages of CCR3+ cells in CSF CD4+ and CD8+ cells increased after the therapy.

3.3. Intracellular TH1/TH2-associated cytokines (Fig. 1)

The IFN-α therapy significantly decreased the ratio of intracellular IFN-γ- versus IL-4-producing T cells in blood (9.5 ± 7.6 before the therapy and 5.8 ± 4.9 after the therapy). The ratios in the three patients who clinically improved following the therapy (Patients HAM 3, 5 and 6) were over 5.0, while the therapy was not effective in any of the four patients with the ratios being less than 5.0 (Patients HAM 9, 4, 1 and 7).

3.4. HTLV-I proviral load (Fig. 2)

The HTLV-I proviral copy number before the IFN-α therapy in the nine patients was 13272 ± 9006 copies and

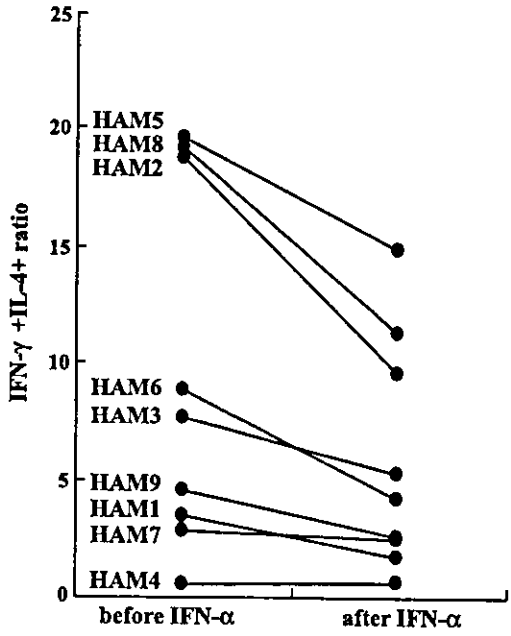

Fig. 1. Intracellular Th1/Th2 cytokine balance in T cells of the patients with HAM/TSP treated with IFN-α. The ratio of IFN-γ+ cells to IL-4+ cells among CD3+ T cells was significantly lower after the IFN-α therapy. Before-IFN-α, before IFN-α therapy; after-IFN-α, after IFN-α therapy.

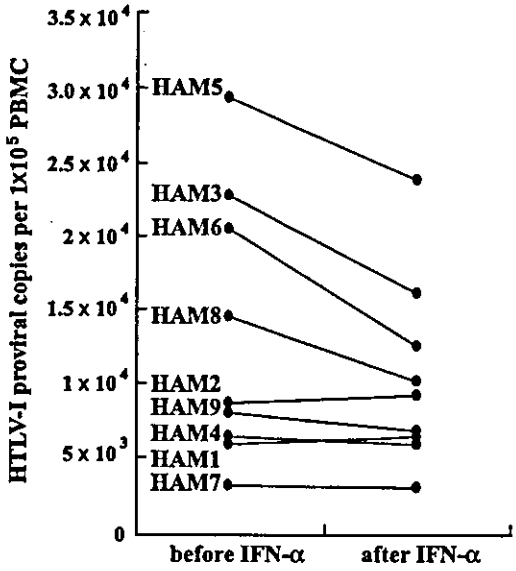

Fig. 2. HTLV-I proviral loads in the PBMC of the patients with HAM/TSP treated with IFN-α. After the IFN-α therapy, HTLV-I proviral loads apparently decreased in the patients with higher proviral loads, and clinical effect was seen in the three patients with 2×10^4 copies or more in 10^5 PBMC (HAM3, HAM5 and HAM6). Before-IFN-α, before IFN-α therapy; after-IFN-α, after IFN-α therapy.

that after the therapy was 10472 ± 6323 copies ($P=0.06$). Patients HAM 3, 5, 8 and 6, who had the highest proviral loads and who experienced the most obvious decline in proviral load as a result of therapy, were among the ones with the highest baseline ratios of intracellular IFN-γ- versus IL-4-producing blood T cells and with the most dramatic decline in those values following the therapy (Fig. 1). Furthermore, three of these four patients were the ones who clinically improved, and all the three patients had 2×10^4 HTLV-I copies or more in 10^5 PBMC. Meanwhile, clinical effect was not seen in any patient with lower HTLV-I proviral load and their proviral loads remained unchanged after the therapy (Fig. 2).

3.5. Correlation

None of the correlations in clinical disability, immunological and virological parameters in the HAM/TSP patients was statistically significant.

3.6. Comparison of immunological and virological findings in responders and non-responders to IFN-α therapy

We compared the immunological and virological findings in responders (Patients HAM 3, 5 and 6) and non-responders (Patients HAM 1, 2, 4, 7, 8 and 9) to the IFN-α therapy (Table 2). We could not analyze the data statistically due to the small sample size. However, among the significant parameters in the statistical analyses of HAM/TSP patients, there was a tendency for the percentages of CCR5+ cells in CD4+ cells in the CSF and blood, the ratio of intracellular IFN-γ- versus IL-4-producing T cells in blood, and the HTLV-I proviral load to be higher and reduce more evidently following the therapy in responders as compared with non-responders. In the other parameters, the percen-

Table 2
Immunological and virological data in "responders" and "non-responders" to the interferon-α therapy

	CCR5+ in CD4+ (%)	CXCR3+ in CD4+ (%)	CCR3+ in CD4+ (%)	CCR5+ in CD8+ (%)	CXCR3+ in CD8+ (%)	CCR3+ in CD8+ (%)	IFN-γ/ IL-4 ratio	HTLV-I proviral load (copies/10^5 PBMC)
Blood								
Responders								
(A) Before therapy	2.0 ± 1.1	28.7 ± 7.8	0.4 ± 0.1	5.6 ± 7.6	49.1 ± 21.2	0.5 ± 0.1	11.8 ± 6.1	24156 ± 4666
(B) After therapy	1.1 ± 0.3	23.3 ± 4.8	0.4 ± 0.2	2.1 ± 1.0	37.2 ± 17.4	0.6 ± 0.4	6.4 ± 2.9	17506 ± 5694
(A)–(B)	0.9 ± 0.4	6.4 ± 7.6	0.0 ± 0.1	3.5 ± 6.6	11.8 ± 4.0	0.1 ± 0.2	5.4 ± 3.5	6650 ± 1107
Non-responders								
(A) Before therapy	1.2 ± 0.8	26.1 ± 10.9	0.4 ± 0.1	1.7 ± 1.7	51.2 ± 19.0	0.8 ± 0.5	8.3 ± 8.7	7830 ± 3802
(B) After therapy	1.0 ± 1.0	26.0 ± 8.8	0.4 ± 0.1	1.3 ± 1.0	37.4 ± 17.6	0.5 ± 0.1	5.6 ± 5.9	6954 ± 2538
(A)–(B)	0.4 ± 0.2	2.4 ± 3.2	0.1 ± 0.2	0.5 ± 0.0	13.8 ± 10.1	0.2 ± 0.5	2.7 ± 3.0	876 ± 1851
CSF								
Responders								
(A) Before therapy	33.5 ± 9.0	92.7 ± 0.8	8.8 ± 5.7	35.4 ± 17.1	97.8 ± 3.1	6.1 ± 2.8		
(B) After therapy	19.4 ± 3.0	89.5 ± 3.2	9.0 ± 4.6	25.4 ± 19.7	96.8 ± 0.5	7.5 ± 1.4		
(A)–(B)	14.1 ± 5.9	3.1 ± 4.0	−0.2 ± 1.1	9.9 ± 19.0	1.0 ± 2.6	−1.5 ± 1.3		
Non-responders								
(A) Before therapy	15.3 ± 2.0	86.8 ± 5.6	2.1 ± 0.6	23.9 ± 9.9	93.6 ± 4.5	3.1 ± 2.9		
(B) After therapy	10.9 ± 4.0	78.0 ± 13.2	6.1 ± 0.2	15.9 ± 5.3	87.9 ± 9.0	7.6 ± 5.0		
(A)–(B)	4.2 ± 2.4	8.8 ± 17.4	−4.5 ± 0.4	8.9 ± 12.2	5.8 ± 11.2	−4.8 ± 6.2		

Data are shown as mean ± standard deviation.
IFN-γ, interferon-gamma; IL-4, interleukin-4; IFN-γ/IL-4, ratio of IFN-γ producing cells to IL-4 producing cells in CD3+ cells; PBMC, peripheral blood mononuclear cells; CSF, cerebrospinal fluid.

tages of CCR3+ cells in CSF CD4+ and CD8+ cells tended to be lower and increase more after the therapy in non-responders than in responders.

4. Discussion

Our previous analysis revealed a significant reduction of CD4+ cells in CSF of HAM/TSP after IFN-α therapy (Feng et al., 2003). In the present study, we focused on the Th1/Th2 balance and showed that IFN-α therapy significantly reduced CCR5+CD4+ cells, a Th1 subset, in the patients' CSF as well as blood. The CCR5+CD4+ cell subset in CSF reflects the disease activity in multiple sclerosis (Misu et al., 2001). This subset is increased in the synovium of active rheumatoid arthritis (Mack et al., 1999), and the inhibition of CCR5 successfully treated adjuvant arthritis in rats, an animal model of rheumatoid arthritis (Barnes et al., 1998). In HAM/TSP, elevated levels of CCR5 on memory CD4+ cells in PBMC (Wu et al., 2000) and macrophage inflammatory protein-1α, a CCR5 ligand, in CSF (Miyagishi et al., 1995) were reported. These findings suggest a pathogenic role of CCR5+CD4+ cells in HAM/TSP and other immunologic diseases, and a suppression of the subset by IFN-α might relate to the alleviation of myelitis in HAM/TSP.

There was also a tendency for the CXCR3+CD4 cell, another Th1 subset, to be decreased and CCR3+CD4+ cells, a Th2 subset, to be increased in CSF of the treated patients. A significant decrease in blood CD8+ cell number in the treated patients (Feng et al., 2003) may be attributable to the reduction in CXCR3+CD8+ cells. Moreover, intracellular Th1/Th2-associated cytokine ratio in T cells, which was analyzed only in blood because of the limited volumes of CSF, reduced significantly following the therapy. Taken together, our data suggests that the IFN-α therapy suppressed Th1-related responses in HAM/TSP, although our small-scale study did not address whether the immunological changes were directly associated with the clinical efficacy of IFN-α in HAMTSP.

The present study suggested some interesting differences in baseline immunological and virological findings between responders and non-responders to the IFN-α therapy, that is, responders showed higher Th1 responses and more viral replication than non-responders, and the therapeutic suppression to those parameters was more evident in responders. Our small-scale study could not confirm the associations statistically, but those analyses will be critically important to reliably predict therapeutic efficacy of intramuscular injections of IFN-α beforehand. Whether such laboratory data as (1) baseline percentage of CCR5+ cells in CSF CD4+ cells >20%, (2) baseline ratio of intracellular IFN-γ- versus IL-4-producing blood T cells >5.0 and (3) baseline HTLV-I proviral load more than one copy in five PBMC are really linked to clinical efficacy of IFN-α therapy in HAM/TSP need to be examined in a larger cohort of patients by statistical analyses.

Acknowledgements

The authors thank Mr. Brent Bell for reading the manuscript. This work was supported by the grants from the Ministry of Education, Science, Culture, Sports and Technology and the Tawara's Endowment for HAM Research.

References

Barnes, D.A., Tse, J., Kaufhold, M., Owen, M., Hesselgesser, J., Strieter, R., Horuk, R., Perez, H.D., 1998. Polyclonal antibody directed against human RANTES ameliorates disease in the Lewis rat adjuvant-induced arthritis model. J. Clin. Invest. 101, 2910–2919.

Feng, J., Misu, T., Fujihara, K., Saito, H., Takahashi, T., Kohnosu, T., Shiga, Y., Takeda, A., Sato, S., Takase, S., Itoyama, Y., 2003. Interferon-alpha significantly reduces cerebrospinal fluid CD4 cell subsets in HAM/TSP. J. Neuroimmunol. 141, 170–173.

Gessain, A., Barin, F., Vernant, J.C., Gout, O., Maurs, L., Calender, A., de The, G., 1985. Antibodies to human T-lymphotropic virus type-I in patients with tropical spastic paraparesis. Lancet 2, 407–410.

Itoyama, Y., Kira, J., Fujii, N., Goto, I., Yamamoto, N., 1996. Increases in helper inducer T cells and activated T cells in HTLV-I-associated myelopathy. Ann. Neurol. 26, 257–262.

Izumo, S., Goto, I., Itoyama, Y., Okajima, T., Watanabe, S., Kuroda, Y., Araki, S., Mori, M., Nagataki, S., Matsukura, S., Akamine, T., Nakagawa, M., Yamamoto, I., Osame, M., 1996. Interferon-alpha is effective in HTLV-I-associated myelopathy: a multicenter, randomized, double-blind, control trial. Neurology 46, 1016–1021.

Izumo, S., Umehara, F., Osame, M., 2000. HTLV-I-associated myelopathy. Neuropathology 20, S65–68 (Suppl).

Jacobson, S., Levin, M., Utz, U., Drew, P., 1998. Infectious immune disorders: HTLV-I. In: Antel, J.P., Birnbaum, G., Hartung, H.P. (Eds.), Clinical neuroimmunology. Blackwell, Malden, pp. 204–217.

Kuroda, Y., Matsui, M., 1993. Cerebrospinal fluid interferon-gamma is increased in HTLV-I-associated myelopathy. J. Neuroimmunol. 42, 223–236.

Mack, M., Bruhl, H., Gruber, R., Jaeger, C., Cihak, J., Eiter, V., Plachy, J., Stangassinger, M., Uhlig, K., Schattenkirchner, M., Schlondorff, D., 1999. Predominance of mononuclear cells expressing the chemokine receptor CCR5 in synovial effusions of patients with different forms of arthritis. Arthritis Rheum. 42, 981–988.

Misu, T., Onodera, H., Fujihara, K., Matsushima, K., Yoshie, O., Okita, N., Takase, S., Itoyama, Y., 2001. Chemokine receptor expression on T cells in blood and cerebrospinal fluid at relapse and remission of multiple sclerosis: imbalance of Th1/Th2-associated chemokine signaling. J. Neuroimmunol. 114, 207–212.

Miyagishi, R., Kikuchi, S., Fukazawa, T., Tashiro, K., 1995. Macrophage inflammatory protein-1 alpha in the cerebrospinal fluid of patients with multiple sclerosis and other inflammatory neurological diseases. J. Neurol. Sci. 129, 223–227.

Nagai, M., Usuku, K., Matsumoto, W., Kodama, D., Takenouchi, N., Moritoyo, T., Hashiguchi, S., Ichinose, M., Bangham, C.R., Izumo, S., Osame, M., 1998. Analysis of HTLV-I proviral load in 202 HAM/TSP patients and 243 asymptomatic HTLV-I carriers: high proviral load strongly predisposes to HAM/TSP. J. Neurovirol. 4, 586–593.

Osame, M., Usuku, K., Izumo, S., Ijichi, N., Amitani, H., Igata, A., Matsumoto, M., Tara, M., 1986. HTLV-I associated myelopathy, a new clinical entity. Lancet 1, 1031–1032.

Pala, P., Hussell, T., Openshaw, P.J., 2000. Flow cytometric measurement of intracellular cytokines. J. Immunol. Methods 243, 107–124.

Umehara, F., Izumo, S., Ronquillo, A.T., Matsumuro, K., Sato, E.,

Osame, M., 1994. Cytokine expression in the spinal cord lesions in HTLV-I-associated myelopathy. J. Neuropathol. Exp. Neurol. 53, 72–77.

Wu, X.M., Osoegawa, M., Yamasaki, K., Kawano, Y., Ochi, H., Horiuchi, I., Minohara, M., Ohyagi, Y., Yamada, T., Kira, J.I., 2000. Flow cytometric differentiation of Asian and Western types of multiple sclerosis, HTLV-I-associated myelopathy/tropical spastic paraparesis (HAM/TSP) and hyperIgEaemic myelitis by analyses of memory CD4 positive T cell subsets and NK subsets. J. Neurol. Sci. 177, 24–31.

Available online at www.sciencedirect.com
SCIENCE DIRECT
Microbes and Infection 6 (2004) 715–724
Microbes and Infection
www.elsevier.com/locate/micinf

Original article

Role of Nup98 in nuclear entry of human immunodeficiency virus type 1 cDNA

Hirotaka Ebina [a], Jun Aoki [a], Shunsuke Hatta [a], Takeshi Yoshida [a], Yoshio Koyanagi [b,*]

[a] *Department of Virology, Tohoku University Graduate School of Medicine, Sendai 980-8575, Japan*
[b] *Laboratory of Viral Pathogenesis, Institute for Virus Research, Kyoto University, 53 Shougoin-kawahara machi, Sakyou-ku, Kyoto 606-8507, Japan*

Received 18 February 2004; accepted 7 April 2004

Available online 24 May 2004

Abstract

Human immunodeficiency virus type 1 (HIV-1), like other lentiviruses, can infect non-dividing cells. The lentiviruses are most likely to have evolved a nuclear import strategy to import HIV-1 cDNA and viral protein complex through the nuclear pore complex (NPC) formed by nucleoporin proteins (Nup). In this study, we found that synthesis of integrated and 2LTR but not full-length form of HIV-1 cDNA was clearly impaired in culture via transduction of vesicular stomatitis virus matrix protein (VSV M), an inhibitor protein, through binding to the phenylalanine-glycine (FG) repeat region of Nup98. The impairment of synthesis of integrated and 2LTR DNA with VSV M was restored by ectopic overexpression of Nup98. A series of experiments using Nup98-depleted NPC by the small interfering RNA (siRNA) technique showed specific impairment of NPC structure and some functions, including nuclear import of HIV-1 cDNA. Our results suggest that Nup98 on the NPC specifically participates in the nuclear entry of HIV-1 cDNA following HIV-1 entry.

Keywords: Nucleoporin; NPC; HIV-1; Nuclear import

1. Introduction

The Retroviridae family of viruses can reverse transcribe their RNA genome into cDNA and then integrate the cDNA into host chromosomes. The lentiviruses (e.g. HIV) are distinguished by their ability to infect non-dividing cells, whereas the gamma-retroviruses (e.g. Moloney murine leukemia virus) require nuclear membrane dissolution to access the host cell DNA [1]. Thus, the lentiviruses are most likely to have evolved a nuclear import strategy, which allows their cDNA to cross the nuclear membrane independently of mitosis. In the case of human immunodeficiency virus type 1 (HIV-1), mitosis-independent replication was initially shown in terminally differentiated macrophages in vitro [1–3]. The mitosis-independent replication of HIV has also enabled the generation of integration-competent gene transfer vectors with promising therapeutic applications in a variety of non-dividing cellular hosts, including neurons [4], myocytes [5], and retinal cells [6]. To facilitate integration into a host DNA, a preintegration complex (PIC) is generated in the cytoplasm immediately after completion of reverse transcription. The PIC can be isolated successfully from in vitro freshly HIV-1-infected or HIV vector-infected cells and was recently shown to have the ability to traverse the nuclear pore complex (NPC) [1,7]. The NPCs serve as the conduits for bi-directional transport of macromolecules. Translocation across the NPC into the nucleus and from the nucleus into the cytoplasm is governed by a class of proteins known as importins and exportins (transport receptors), respectively. Both are members of the karyopherin family. The transport receptors engage the appropriate import or export signals and mediate their transport [8,9]. The PIC contains a double-strand linear cDNA as well as at least four viral proteins: matrix (MA), reverse transcriptase (RT), integrase (IN), and viral protein R (VPR), and has a diameter of approximately 56 nm, which greatly exceeds the 25 nm central channel of the NPC [1,7,10]. The NPC has a large supramolecular structure formed of ~50 unique proteins in eukaryotic cells, termed nucleoporins (Nup) [8,9,11,12]. High-resolution electron microscopic images of NPCs reveal an eightfold

* Corresponding author. Tel.: +81-75-751-4811; fax: +81-75-751-4812.
E-mail address: ykoyanag@virus.kyoto-u.ac.jp (Y. Koyanagi).

doi:10.1016/j.micinf.2004.04.002

symmetric structure, formed by nuclear and cytoplasmic rings and central spoke complex. The Nups often contain multiple phenylalanine-glycine (FG) dipeptide repeats clustered in domains, which in vertebrates are glycosylated by addition of *O*-linked *N*-acetylglucosamine (GlcNAc). Some of these Nups are localized asymmetrically at the NPC [9,11]. The asymmetric distribution of nucleoporins and the different affinities for import and export complexes may be important in determining the direction of transport [13,14]. Recent studies reported that importin 7 is involved in the nuclear entry of HIV-1 PIC as one of the main transport receptors [15]. However, the steps involved in the NPC remain largely undefined. In the present study, we show that nuclear import of HIV-1 cDNA requires NPC, and Nup98 has a role in nuclear entry of HIV-1 cDNA.

2. Materials and methods

2.1. Chemical treatment

Aphidicolin (APH) (Sigma Chemical Co., St. Louis, MO, USA), actinomycin D (ActD) (Sigma), zidovudine (AZT) (Sigma) or leptomycine B (LMB) (Sigma) was used. APH treatment (5 μg/ml) started 24 h before HIV-1 vector infection. AZT treatment started at the time of infection. LMB was added 2 h after infection. ActD was added 5 h after infection. DNA was extracted 24 h after infection.

2.2. Transfection

Human 293T cells were maintained in D-MEM containing 10% fetal calf serum (FCS). 293T cells were transfected with vesicular stomatitis virus matrix protein (VSV M)-, Nup98- or small interfering RNA (siRNA)-expressing DNA using calcium phosphate methods.

2.3. Quantitative polymerase chain reaction (PCR) assay

For the detection and quantification of individual forms of HIV-1 DNA, full-length/1LTR circle, 2LTR circle and integrated forms, we used a set of primer pairs and fluorogenic probes, as described previously [16,17]. PCR was performed using an ABI PRISM 7700 sequence detection system (PE-Applied Biosystems, Foster City, CA, USA) and TaqMan Universal PCR Master Mix (PE-Applied Biosystems). Cycling conditions included a hot start (50 °C for 2 min, 95 °C for 10 min), followed by 40 cycles of denaturation (95 °C for 15 s) and extension (60 °C for 1 min). To measure the integrated DNA, an *Alu*-sequence-specific sense primer and an antisense HIV-specific primer were used in the first PCR and subsequently 1000-fold diluted products were subjected to real-time PCR assay for measurement of R/U5 DNA, as described previously [16,17].

2.4. Cell-cycle analysis

Cell-cycle progression was examined by single-color flow cytometric analysis of the DNA content stained with 50 μg/ml of propidium iodine (Sigma).

2.5. DNA constructs and recombinant protein expression

Small interference RNA (siRNA)-expressing plasmid DNAs were constructed using the method described by Miyagishi and Taira [18]. The sequences inserted in the *Bfu*AI site of pU6i cassette, immediately downstream of the U6 promoter, were as follows: Nup98-targeted siRNA (siN98), 5′-CACC**GAATATGAAAG*T*AAGTT*A*TT**ATAGAATTACATCAAGGGAGATTAGTGACTTGCTTTCATATTCTTTTTATGC-3′; firefly luciferase-targeted siRNA (siLuc), 5′-CACC**GTGCG*T*TG*T*TGGTG*TT*AA*T*CC**ATCTCCCTTGATGTAATTCTAGGGTTGGCACCAGCAGCGCACTTTTTATGC-3′. Bold-lettered nucleotides are the siRNA sequences, italic nucleotides are mutated, and underlined nucleotides are loop sequences. The siRNA-expressing DNA fragment was also inserted into the *Eco*RI site of a lentivirus vector DNA, pCS-CDF-EH2K^k, and an enhanced green fluorescence protein (EGFP) fragment between the *Age*I and *Xho*I sites of pCS-CDF-EG-PRE [19] was replaced with a H-2K^k fragment (Daiichi pure chemicals, Tokyo, Japan).

HA-tagged human Nup98-expressing plasmid DNA (p37R-HANup98) and EGFP-fused VSV M-expressing DNA (pEGFPN3-M) [20] were kindly provided by Dr. Elisa Izaurralde (European Molecular Biology Laboratory). A *Bss*HII-*Xho*I DNA fragment covering the coding region of HA-tagged human Nup98 region was cloned into a site downstream of CMV promoter in pcDNA3.1/Zeo (+) (Invitrogen, Carlsbad, CA, USA) (pcDNup98). Alanine substitutions from Asp-Thr-Tyr at the position of VSV M 52–54 [VSV (M)] were introduced using an oligonucleotide-directed in vitro mutagenesis system (Quickchange site-directed mutagenesis, Stratagene, San Diego, CA, USA). DsRed-fusion recombinant protein with NLS, U1A and rpL23a was produced in *Escherichia coli*. A double-strand synthetic nucleotide of SV40 NLS (5′-CCA TGC ATA TGC CAA AAA AGA AGA GAA AGG TTG-3′) and PCR-amplified DNA fragment of U1A (1–486), or rpL23a (1–486) from mRNA of HeLa cells was cloned into the *Sma*I or *Sal*I-*Bam*HI sites of pDsRed1-N1 (Clontech, Palo Alto, CA, USA), and then a *Sal*I-*Not*I fragment was inserted in the *Sal*I-*Not*I site of pGEX-4T-2 (Amersham Pharmacia Biotech, Piscataway, NJ, USA). *E. coli* ER2566 (New England Biolabs Inc., Beverly, MA, USA) was used, and recombinant proteins were purified on glutathione sepharose 4 Fast Flow (Amersham) by standard protocols, as previously described [21].

2.6. Reverse-transcription PCR

Total RNA was extracted from transiently transfected cells by using a RNeasy RNA-preparation Kit (Qiagen, KJ

Venlo, The Netherlands). Reverse transcription and PCR were carried out using a SuperScript One-Step RT-PCR with Platinum Taq (Invitrogen). We used the following primers to detect the specific transcripts: for Nup107, 5′-AAACGCG-GTAGCTAAACTGCA-3′, 5′-ACCACCAGCTGACTT-TGTCGA-3′; for Nup214, 5′-CTTGCCACGAAAAC-CGTGA-3′, 5′-CAACCCGCAGTCCTGAAAA-3′; for p62, 5′-CAGACACCGACGGATTTGCTT-3′, 5′-TGGATGTTG-TTGTGGAGGTGC-3′; for Nup98, 5′-TCTCATCCCAA-AACAATGCCTT-3′, 5′-AAACAAAGATGCCTGTCC-AGCA-3′; for Nup153, 5′-TGACAATGAAGAGCC-AAAGTGT-3′, 5′-TAGGAGTTGTTCCAGAGCCAAA-3′. TaqMan GAPDH Control Reagents (PE-Applied Biosystems) were used as primer sets for glyceraldehyde 3-phosphate dehydrogenase (GAPDH). Fifty nanograms of template RNA and 10 pmol of specific primers were used. The efficiency of PCR amplification was roughly in the linear range, as determined by preliminary test with increasing number of cycles. Finally, the PCR products were analyzed by agarose gel electrophoresis using standard techniques.

2.7. Virus vector infection

For HIV-1 vector preparation, a replication-incompetent EGFP-expressing lentivirus (pCS-CDF-CG-PRE) or siRNA-expressing lentivirus was co-transfected into 293T cells along with VSV G-expressing plasmid (pVSV G), HIV-Gag-Pol-expressing plasmid (pRRE) and Rev-expressing plasmid (pRSV-Rev) as described before [6,19]. Three days after transfection, the culture supernatants were cleared by filtration and concentrated through centrifugation at 6000 × *g* for 16 h at 4 °C. The transducing unit (TU) was determined by measurement of EGFP-, or H-2K^k-expressing cells using flow cytometry. Phycoerythrin-labeled anti-mouse H-2K^k monoclonal antibody (mAb) (Cedarlane, Ontario, Canada) was used. Cells were analyzed on FACS SCAN, using Cell Quest software (BD PharMingen, San Diego, CA, USA). Treatment with DNaseI (20 μg/ml) was performed to remove plasmid DNA in the virus stocks. Heat-inactivated (65 °C, 30 min) virus liquid was used as negative control for HIV DNA quantification in infected cells. APH-treated MT-2 cells or 293T cells (2×10^5 cells) were infected with HIV-1 vector (4×10^5 TU). Two hundred thousand 293T cells were transfected with VSV M- or Nup98-expressing DNA and then 24 h later, infected with HIV-1 vector (4×10^5 TU). Two hundred thousand 293T cells were transfected with siRNA-expressing DNA and then 72 h later, infected with HIV-1 vector (4×10^5 TU). The amount of viral DNA was measured by the quantitative PCR assay 24 h after infection, as described above. HeLa cells (1×10^5 cells), grown on cover-slips, were infected with siRNA-expressing HIV-1 vector at multiplicity of infection (m.o.i.) of 1. The cells were analyzed 96 h later by immunofluorescence, immunoblotting or nuclear import assay.

2.8. Immunofluorescence analysis

HeLa cells, grown on cover-slips, were washed twice with phosphate-buffered solution (PBS) and fixed in 4% (vol/vol) paraformaldehyde/PBS for 15 min at room temperature. The cells were permeabilized with 0.2% Triton X-100/PBS for 5 min. After blocking with 5% bovine serum albumin (BSA)/0.1% Triton X/PBS for 1 h, the cells were incubated with an NPC-specific mouse mAb, mAb414 (BabCO, Berkeley, CA, USA) or anti-Nup98 polyclonal antibody (C-16) (Santa Cruz Biotechnology Inc., Santa Cruz, CA, USA) at 4 °C overnight. Cells were washed three times with 0.05% Triton X/PBS and then incubated with Alexa 594-conjugated goat anti-mouse IgG antibody (Molecular Probes, Eugene, OR, USA) or fluorescein isothiocyanate (FITC)-conjugated donkey anti-goat IgG antibodies (Chemicon, Temecula, CA, USA) for 1 h. Cells were washed three times with 0.05% Triton X/PBS, mounted in Vectashield mounting medium for fluorescence (Vector Laboratories, Burlingame, CA, USA) and analyzed with a Leica QFluoro system. The cells were also stained with Hoechst 33342 (Molecular Probes).

2.9. Nuclear import assay

HeLa cells grown on cover-slips were washed in PBS and permeabilized for 5 min on ice in 50 μg/ml digitonin (Sigma)/transport buffer (20 mM Hepes– NaOH, pH 7.3, 110 mM CH_3COOK, 2 mM $(CH_3COO)_2Mg$, 5 mM CH_3COONa, and 2 mM dithiothreitol). After washing three times with transport buffer, cells were incubated at 30 °C for 30 min in the presence of energy-regenerating system (1 mM ATP, 1 mM GTP, 10 mM creatine phosphate, and 20 U/ml creatine phosphokinase), 3 μM DsRed-labeled recombinant protein, and cytoplasmic extract from 2×10^5 HeLa cells. Samples were washed three times in transport buffer, fixed on ice for 30 min with 1% formalin/transport buffer and analyzed with a Leica QFluoro system.

2.10. Immunoblotting

293T cells were co-transfected with an HA-tagged human Nup98-expressing plasmid DNA (pcDNup98) and a siRNA-expressing plasmid (siN98 or siLuc). Three days after transfection, the cells were washed twice and lysed in RIPA buffer (0.5% NP-40 in 20 mM Tris–HCl [pH 8.2], 0.15 M NaCl, 5 mM iodoacetamide, and 1 mM phenylmethylsulfonyl fluoride). After loading on SDS/PAGE, polypeptides were transferred to Immobilion Transfer Membranes (Millipore, Billerica, MA, USA), the level of Nup98 was determined using a goat anti-Nup98 polyclonal antibody (C-16), biotin-conjugated rabbit anti-goat IgG (Chemicon) and then incubated with horseradish peroxidase (HRP)-conjugated streptavidin (Zymed, San Francisco, CA, USA). The filter generated from HeLa cells infected with siRNA-expressing

HIV-1 vector as described above was also incubated with mAb414 (mainly reactive against p62), biotin-conjugated horse anti-mouse IgG (VECTOR) and HRP-conjugated streptavidin. The specific bands were detected using Western Lighting Chemiluminescence Reagent (Perkin–Elmer Life Science, Boston, MA, USA). For detection of Nup98-VSV M complex, 293T cells were co-transfected with Nup98-expressing plasmids (pcDNup98) and EGFP-fused VSV M-expressing plasmid DNA (pEGFPN3-M) or the mutant [VSV M(D)]. Two days after transfection, the cells were lysed in triple detergent lysis buffer (1% NP-40, 0.1% SDS, 0.5% sodium deoxycholate in 50 mM Tris–HCl [pH 8.0], 0.15 M NaCl, 1 μg/ml aprotinin, 1 mM phenylmethylsulfonyl fluoride), and a mouse anti-HA mAb (F-7) (Santa Cruz) was added. After incubation for 12 h at 4 °C with protein G-sepharose (Amersham), the precipitate was washed three times with triple detergent lysis buffer, and the bound proteins were eluted by 1× sample buffer (1.71% SDS in 175 mM Tris–HCl [pH 6.8], 5% glycerol, 1% 2-mercaptoethanol) at 37 °C for 30 min. The samples were loaded on SDS/PAGE and transferred to Immobilon Transfer Membranes. For detection of the Nup98, a goat anti-Nup98 polyclonal antibody (C-16) (Santa Cruz) and biotin-conjugated rabbit anti-goat IgG (Chemicon) were used. For detection of VSV M, a rabbit anti-GFP polyclonal antibody (Santa Cruz) and biotin-conjugated donkey anti-rabbit IgG (Chemicon) were used.

2.11. Statistical analysis

All data were expressed as mean ± standard deviations (S.D.). Differences between groups were examined for statistical significance using the Welch's *t*-test. A P value less than 0.05 denoted the presence of a statistically significant difference.

3. Results

3.1. Efficient nuclear import of HIV-1 cDNA in infected cells

It has been shown that HIV and HIV-based lentivirus vectors efficiently infect non-dividing cells [2,6]. To determine the integration efficiency in dividing and non-dividing cells, we prepared cell-cycle-arrested T cell culture using MT-2 cells treated with APH, an inhibitor of DNA polymerase α. Under this condition, cell-cycle was confirmed to be stopped at G1 phase from flow cytometric analysis (Fig. 1A). The same numbers of treated (arrested) or untreated (proliferating) cells were infected with the same amounts of HIV-1 vector and the arrested culture was further maintained in the presence of APH. Since in this experiment we used a single-round infection system, we could estimate the precise efficiency of reverse transcription, nuclear translocation as well as integration. Total DNA was extracted 24 h after infection and a set of real-time PCR assay was performed [16,17]. Using this assay, we were able to measure the full-length/1LTR circle, 2LTR circle and integrated forms of HIV-1 cDNA, respectively. Since the 2LTR circle and integrated forms are found only in nucleus after HIV infection [3,22], we could estimate the efficiency of nuclear entry as well as integration of HIV-1 cDNA. Fig. 1B shows that the levels of integrated, 2LTR and full-length/1LTR circle form in proliferating cultures were higher than those in arrested cultures, because the numbers of the cells were two to three times greater in proliferating culture. However, significant amounts of integrated ($4.2 \times 10^5 \pm 5.4 \times 10^4$ copies per culture) and 2LTR ($1.5 \times 10^5 \pm 1.5 \times 10^3$ copies per culture) form DNA were found in the arrested culture (Fig. 1B). Similar results were also obtained in APH-treated 293T cells (data not shown). These data correspond well with the previously reported findings of the high susceptibility of APH-treated cells to HIV-1 [3,22]. Importantly, the ratios of integrated form and 2LTR form to full-length/1LTR form were similar in the proliferating (integrated; 0.108 ± 0.024, 2LTR; 0.022 ± 0.002, full-length/1LTR; 1.0) and the arrested cultures (integrated; 0.09 ± 0.011, 2LTR; 0.031 ± 0.001, full-length/1LTR; 1.0), respectively, strongly suggesting that HIV-1 cDNA efficiently traverse NPC, depending on the active nuclear import machinery in not only non-dividing cells but also proliferating cells.

3.2. Inhibition of HIV-1 cDNA import with a Nup98-specific inhibitor

Next, to examine the specificity of our real-time PCR assay and the associated molecules in nuclear entry of HIV-1 cDNA, we prepared HIV reverse transcription-inhibited (AZT-treated), transcription-blocked (ActD-treated), or CRM1-dependent nuclear export-inhibited (LMB-treated) 293T cell cultures. As expected, AZT significantly inhibited the appearance of all forms of DNA (Fig. 2A a–c). Although dose-dependent inhibition of integration was found in ActD- or LMB-treated cultures, significant accumulation of the 2LTR form was also found (Fig. 2A f and i), suggesting that newly synthesized proteins as well as CRM1-dependent exported proteins may be required for the efficient integration but not nuclear entry of HIV-1 cDNA. To examine whether specific Nups are required for HIV infection, we used VSV M protein, a specific inhibitor protein against Nup98. It has been shown that Nup98 is involved in the nuclear import of some proteins as well as the export of RNA, and its function is specifically impaired in the presence of VSV M protein [20]. The VSV M binds a region within residues 66–515 of Nup98 that encompasses most of the FG repeats, the hRAE1/Gle2 binding site or GLEBS-like motif [23], and most of the predicted glycosylation sites of the Nups. Through these sites, Nup98 was able to interact with three

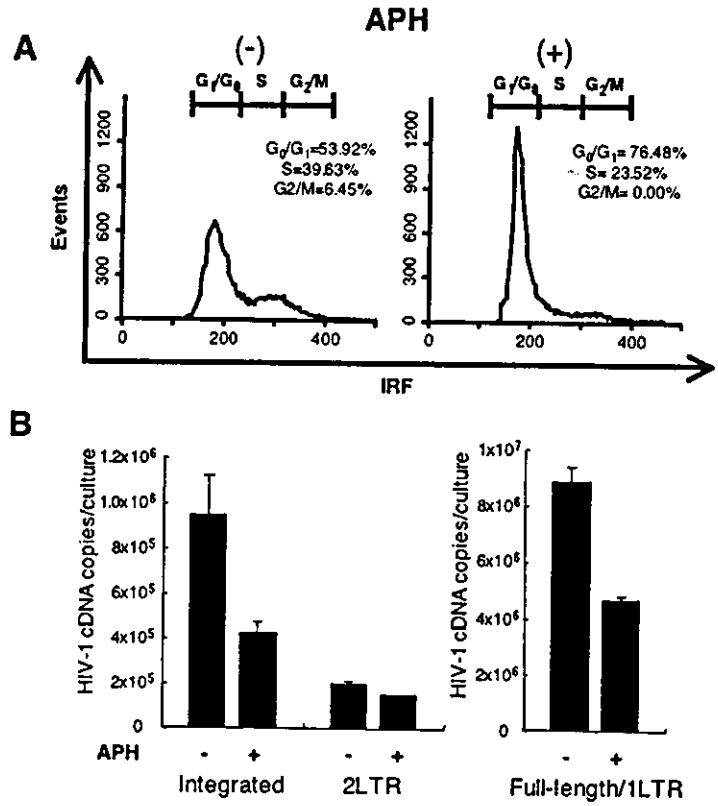

Fig. 1. Efficient nuclear entry of HIV-1 cDNA in arrested cells. (A) Cell-cycle analysis of APH-treated and -untreated cells. MT-2 cells were incubated for 24 h without (–) or with (+) APH, and then analyzed for DNA content by flow cytometry of proridium iodide-stained nuclei. Representative flow cytometry data from one of three independent experiments is shown. (B) Quantification of HIV-1 cDNA after HIV-1 vector infection in APH-treated and -untreated cells. Number of viral DNA copies per culture (baseline cell number is 2×10^5 cells) is indicated. APH-treated or -untreated MT-2 cells were infected with HIV-1 vector, and cultured without (–) or with (+) APH for another 24 h, respectively. Then, DNA was extracted and subjected to PCR assay. Results are mean ± S.D. of three independent experiments.

putative Nup98 partners: RAE1 [23], CRM1 [24], and TAP [25]. VSV M-mediated inhibition was not observed in a site-directed mutant (residue 52–54), termed VSV M(D) [20]. We used the VSV M as a specific inhibitor of the Nup98 function. An obvious impairment of integrated and 2LTR but not full-length DNA was found in only the wild-type but not the mutant VSV M(D)-transfected culture (Fig. 2B). This impairment was restored with ectopic overexpression of Nup98 (pcDNup98) (Fig. 2B, lane 5). Western blotting indicated that the overexpressed Nup98 was co-precipitated with VSV M but not VSV M(D) protein (Fig. 2C), suggesting that the overexpressed Nup98 absorbed VSV M protein, and the Nup98 function was recovered. Thus, Nup98 may have a role in nuclear import of HIV cDNA.

3.3. Depletion of Nup98 by siRNA

Next, to examine directly the involvement of Nup98 in HIV-1 cDNA nuclear import, Nup98 was depleted by the siRNA technique. After transfection with Nup98-specific siRNA-expressing plasmid, mRNA expression of Nup98 as well as Nup96, generated from the same precursor transcripts of Nup98 [26], but not other Nups such as p62, Nup107, Nup153, and Nup214, were specifically inhibited (Fig. 3A). It was also confirmed that the level of ectopic Nup98 protein expression was inhibited with the siRNA-expressing plasmid as it was lower than that in its endogenous expression (Fig. 3B). Immunofluorescence analysis using an anti-Nup98 antibody also confirmed the significant inhibition of Nup98 expression on nuclear membrane in the Nup98 siRNA-targeted HeLa cells using a siRNA-expressing lentivirus vector (Fig. 3C, upper panel). We further examined the distribution of NPC components using mAb414, an antibody known to interact with many FG-containing Nups, mainly p62 and to a less degree, Nup153, Nup214, and Nup358 but not Nup98. The Nup98 siRNA-transduced cells exhibited weak mAb414-labeling intensity at the nuclear rim and shift of labeling to the cytoplasm, probably cytoplasmic annulate lamellae (Fig. 3C, lower panel). However, the total amount of p62 (main component of NPC) was similar in both Nup98-siRNA-targeted or control cultures (Fig. 3D). A previous study using Nup98 knockout mice indicated that Nup98 is essential for rapid cell proliferation but dispensable for basal cell growth and some specific destruction of NPC component [27]. The Nup98-knockout cell was reported to have a thin nuclear envelope as well as many cytoplasmic annulate lamellae. Our Nup98-siRNA-targeted cells had similar structures. It was also reported that the mutant pores of the knockout cells were clearly impaired in in vitro transport